

1 Vaccines combining slow delivery and follicle targeting of antigens increase 2 germinal center B cell clonal diversity and clonal expansion

4 **Authors:** Kristen A. Rodrigues^{1,2,3,4 †}, Yiming J. Zhang^{1,3,4,5 †}, Aereas Aung¹, Duncan M.
5 Morgan^{1,6}, Laura Maiorino^{1,3,4}, Parisa Yousefpour^{1,3,4}, Grace Gibson⁷, Gabriel Ozorowski⁷,
6 Justin R. Gregory^{1,3,4}, Parastoo Amlashi^{1,3,4}, Maureen Buckley^{1,3,4,5}, Andrew B. Ward^{4,7}, William
7 R. Schief^{3,4,8,9}, J. Christopher Love^{1,3,6*}, Darrell J. Irvine^{1,3,4,5,8,10,11*}

8 **Affiliations:**

9 ¹Koch Institute for Integrative Cancer Research, Massachusetts Institute of Technology;
10 Cambridge, MA 02139 USA.

11 ²Harvard-MIT Health Sciences and Technology Program, Institute for Medical Engineering and
12 Science; Massachusetts Institute of Technology, Cambridge, MA 02139 USA.

13 ³Ragon Institute of Massachusetts General Hospital, Massachusetts Institute of Technology and
14 Harvard University; Cambridge, MA 02139 USA.

15 ⁴Consortium for HIV/AIDS Vaccine Development, The Scripps Research Institute; La Jolla, CA
16 92037 USA.

17 ⁵Department of Biological Engineering, Massachusetts Institute of Technology; Cambridge, MA
18 02139 USA.

19 ⁶Department of Chemical Engineering, Massachusetts Institute of Technology; Cambridge, MA
20 02139 USA.

21 ⁷Department of Integrative, Structural and Computational Biology, The Scripps Research
22 Institute; La Jolla, CA 92037 USA

23 ⁸Department of Immunology and Microbiology, The Scripps Research Institute, La Jolla, CA,
24 92037, USA

25 ⁹IAVI Neutralizing Antibody Center, The Scripps Research Institute, La Jolla, CA, 92037, USA

26 ¹⁰Department of Materials Science and Engineering, Massachusetts Institute of Technology;
27 Cambridge, MA 02139 USA.

28 ¹¹Howard Hughes Medical Institute; Chevy Chase, MD 20815 USA.

29 *Corresponding authors. Email: djirvine@mit.edu, clove@mit.edu

30 [†] These authors contributed equally to this work.

31

32 **One Sentence Summary:** Alum-anchored antigen combined with the saponin adjuvant SMNP
33 promotes follicular targeting of antigen and increases clonal expansion and clonal diversity of
34 germinal center responses in mice.

35

36 **Abstract:** (233/250) Vaccines incorporating slow delivery, multivalent antigen display, or
37 immunomodulation through adjuvants have an important role to play in shaping the humoral

38 immune response. Here we analyzed mechanisms of action of a clinically relevant combination
39 adjuvant strategy, where phosphoserine (pSer)-tagged immunogens bound to aluminum hydroxide
40 (alum) adjuvant (promoting prolonged antigen delivery to draining lymph nodes) are combined
41 with a potent saponin nanoparticle adjuvant termed SMNP (which alters lymph flow and antigen
42 entry into lymph nodes). When employed with a stabilized HIV Env trimer antigen in mice, this
43 combined adjuvant approach promoted substantial enhancements in germinal center (GC) and
44 antibody responses relative to either adjuvant alone. Using scRNA-seq and scBCR-seq, we found
45 that the alum-pSer/SMNP combination both increased the diversity of GC B cell clones and
46 increased GC B cell clonal expansion, coincident with increases in the expression of *Myc* and the
47 proportion of S-phase GC B cells. To gain insight into the source of these changes in the GC
48 response, we analyzed antigen biodistribution and structural integrity in draining lymph nodes and
49 found that the combination adjuvant approach, but not alum-pSer delivery or SMNP alone,
50 promoted accumulation of highly intact antigen on follicular dendritic cells, reflecting an
51 integration of the slow antigen delivery and altered lymph node uptake effects of these two
52 adjuvants. These results demonstrate how adjuvants with complementary mechanisms of action
53 impacting vaccine biodistribution and kinetics can synergize to enhance humoral immunity.

54 INTRODUCTION

55 Vaccination elicits robust and targeted protection against infection by prompting the immune
56 system to recognize potential threats (1). Most licensed vaccines are thought to protect through
57 antibody responses (1, 2), whereby antigen-specific helper T cells and B cells are activated and
58 work together in germinal centers (GCs) to generate high-affinity antibody-secreting plasma cells
59 and memory B cells (3). Despite the success of vaccination-induced immunity against many
60 pathogens, a number of major challenges remain, such as the development of effective vaccines
61 against HIV and tuberculosis, “universal” vaccines for influenza that could provide cross-seasonal
62 protection, or pan-coronavirus vaccines (4–7).

63 HIV serves as a useful exemplar of challenges common to these “difficult” vaccine cases:
64 A protective vaccine will likely need to elicit several classes of broadly neutralizing antibodies
65 (bnAbs), which recognize conserved sites on the viral envelope across the diversity of circulating
66 viral strains. HIV-infected humans can generate bnAbs, and many classes of bnAbs have been
67 isolated from patients (8, 9). However, HIV bnAbs have uncommon features such as extensive
68 somatic hypermutation (SHM), improbable mutations, and very long CDR3 junction lengths (10,
69 11). Consequently, bnAb-precursor B cells are typically rare and present at very low frequencies
70 in the human B cell repertoire (12–14).

71 To overcome these challenges, vaccine regimens capable of recruiting rare B cell clones
72 into the GC reaction and promoting their expansion and affinity maturation may be required. One
73 strategy to modulate the GC response is by manipulating vaccine kinetics, i.e. the timing of
74 inflammatory cue or antigen delivery to draining lymph nodes (dLNs). For example, sustained
75 vaccine delivery over a few weeks using repeated injections or implantable osmotic pumps has
76 been shown to increase the number of unique clones recruited to GCs and greatly increase the size
77 of the GC response compared to traditional bolus vaccine administration (15–17). To make this
78 approach more clinically translatable, we converted the most common clinical adjuvant, aluminum
79 hydroxide (alum), into a slow-delivery vehicle by modifying immunogens with short
80 phosphoserine (pSer) peptide tags (18–20). Through a ligand exchange reaction between
81 phosphate and hydroxyls, these pSer tags anchor antigens to the surface of alum particles. This
82 approach, which we refer to hereafter as “alum-pSer”, promotes stable retention of the antigen on
83 alum particles *in vivo* and leads to prolonged antigen drainage from the injection site following a
84 bolus injection, which translated into improved GC B cell and serum IgG antibody responses and
85 the development of long-lived bone marrow plasma cells in mice for HIV and SARS-CoV-2
86 antigens (18–20).

87 A second approach to tune GC responses is via the selection of appropriate adjuvants,
88 which can impact many aspects of the immune response including antigen presentation, immune
89 cell recruitment and retention in dLNs, and inflammatory cytokine production that direct the
90 adaptive immune response (21, 22). Saponins are potent adjuvants for promoting humoral response
91 and are used in the licensed Shingrix® and Mosquirix® vaccines from Glaxo-Smith Kline as well
92 as the Novavax SARS-CoV-2 vaccine (23, 24). We recently developed a saponin-based adjuvant
93 called SMNP, a ~40 nm diameter nanoparticle formed by the self-assembly of phospholipids,
94 cholesterol, saponin, and the Toll-like receptor (TLR)-4 agonist monophosphoryl lipid A (MPLA)
95 (25). SMNP co-administration has multiple effects on the immune response in both mice and non-
96 human primates, including enhanced lymph trafficking of antigen, increased antigen entry into
97 dLNs, and induction of a cascade of inflammatory cytokines and chemokines (17, 25, 26).

98 Based on these promising findings, SMNP will shortly enter first-in-human testing through the
99 HIV Vaccine Trials Network (HVTN 144).

100 Inspired by their complementary mechanisms of action, we previously tested the impact of
101 combining pSer-tagging of antigens for alum anchoring and sustained antigen delivery with co-
102 administration of SMNP. We discovered that this combination adjuvant approach showed striking
103 amplification of humoral responses to both HIV Env and SARS-CoV-2 antigens (19, 20): alum-
104 pSer + SMNP immunization led to enhancements in GC B cell and Tfh responses, and increased
105 serum IgG and neutralizing antibody responses. Here, we sought to investigate the immunological
106 basis of these improved humoral immune responses and identify underlying mechanisms that
107 might explain this striking potency of the alum-pSer/SMNP combination. We first performed
108 single-cell RNA sequencing (scRNA-seq) transcriptional profiling and single-cell B cell receptor
109 sequencing (scBCR-seq) of antigen-binding GC B cells from mice immunized with a stabilized
110 HIV Env trimer immunogen termed MD39 combined with alum-pSer, SMNP, or alum-
111 pSer/SMNP adjuvants. These analyses revealed that the combination adjuvant augmented multiple
112 complementary facets of the GC response and increased the proportion of GC B cells in S phase
113 of the cell cycle, suggesting greater antigen acquisition and T cell help. Motivated by these
114 findings, we analyzed the biodistribution of antigen following alum-pSer, SMNP, or combined
115 adjuvant immunization, and discovered that the combination adjuvants uniquely promoted robust
116 accumulation of intact trimer antigen on follicular dendritic cells (FDCs), which persisted for
117 several weeks. These findings indicate that this simple combination adjuvant approach achieves
118 both sustained antigen availability and altered antigen localization that can productively drive
119 important changes in the composition of the GC response, which may be valuable for diverse
120 infectious disease targets.

121

122 RESULTS

123 scRNA-seq profiling of antigen-specific GC B cells primed by alum-pSer and SMNP 124 immunizations

125 To gain insights into how alum-pSer and SMNP impact the humoral immune response, we first
126 carried out a single-cell RNA-seq (scRNA-seq) study of antigen-binding GC B cells elicited by
127 these adjuvants combined with an HIV Env stabilized SOSIP trimer immunogen termed MD39
128 (27). We compared 3 formulations (**Fig. 1A**): For alum-pSer immunization, a peptide tag
129 containing four pSer residues was conjugated to the C-terminus of each MD39 gp140 protomer,
130 leading to three pSer₄ tags placed at the base of each trimer. When mixed with alum adjuvant, the
131 phosphoserines of these tagged trimers undergo a ligand exchange reaction with hydroxyl groups
132 on the surface of alum, anchoring the trimer immunogen in an oriented fashion to the alum particles
133 (18–20) (alum-pSer, **Fig. 1A**). The second vaccine formulation was comprised of MD39 trimer
134 mixed with SMNP adjuvant (SMNP, **Fig. 1A**). SMNP is composed of ~40 nm particles of saponin,
135 MPLA, lipids, and cholesterol, which self-assemble to form a cage-like structure; SMNP does not
136 interact with the MD39 trimer in solution (**fig. S1**). The third formulation was comprised of the
137 combination of pSer-tagged MD39 bound to alum and mixed with SMNP particles (alum-
138 pSer/SMNP, **Fig. 1A**).

139 We previously found that MD39 + alum-pSer/SMNP elicited antibody and GC B cell
140 responses substantially superior to either alum-pSer or SMNP alone (18, 20). To identify an
141 appropriate timepoint for scRNA-seq analysis, we first immunized BALB/c mice with each

142 formulation and analyzed humoral responses over time (**Fig. 1B-D**). As shown in **Fig. 1B**, GC
143 responses in all 3 groups steadily expanded for two weeks post-immunization, peaking at day 14,
144 and then began contracting. Consistent with our prior findings, there was a clear hierarchy in size
145 of the GC responses, with the combination alum-pSer/SMNP immunization eliciting 1.9-fold and
146 5.6-fold more GC B cells than SMNP or alum-pSer alone, respectively, at the peak of the response.
147 Serum antibody responses developing over the same time course also showed the strongest
148 response in the combination adjuvant group (**Fig. 1C**). Based on these findings, we carried out
149 scRNA-seq and scBCRseq analyses at the peak of the GC response for each group, day 14 post-
150 immunization. Groups of mice were immunized with each of the 3 vaccine formulations, and the
151 antigen-binding GC B cells were flow sorted for combined scRNA-seq and scBCR-seq using
152 SeqWell, a nanowell-based library preparation (28–30) (**Fig. 1D**).

153 The number of recovered cells in each immunization condition reflected the magnitude of
154 the GC response detected by flow cytometry (**Fig. 2A**). After quality control, we recovered the
155 transcriptome of 11,231 MD39-binding GC B cells, including 149 from alum-pSer, 2608 from
156 SMNP, and 8474 from alum-pSer/SMNP immunized mice (**Fig. 2B**). We first examined the
157 transcriptome data. Leveraging unsupervised clustering and differential gene expression analysis,
158 we identified seven phenotypic clusters (**Fig. 2C-D**). Among them, cluster 1 (C1) showed
159 plasmablast gene signatures such as *Cd138* (*Sdc1*), Blimp-1 (*Prdm1*), *Xbp1*, and *Ell2* (31). C2
160 upregulated *Ccr6*, *Hhex*, *Fcer2a*, and GC egressing markers *Itga4*, *Itgb7*, *Lmo2*, and *Cmah*,
161 suggesting that C2 cells are likely GC-derived pre-memory B cells (MBCs) (32–34). C3 cells
162 expressed genes involved in antigen capturing and presentation (*H2-DMa*, *H2-Ab1*, *Ciita*, *Cr2*)
163 and signaling with T cells (*Cd83*, *Cd86*, *Cd40*) (35, 36), implicating a light zone (LZ) B cell
164 phenotype. Cell division is the hallmark of dark zone (DZ) B cells (3, 35). We demarcated DZ
165 cells into three sub-clusters, where C5 was characterized by S phase genes (*Mcm6*, *Pcna*, *Lig1*),
166 C6 by active cycling genes (*Cenpe*, *Mki67*, *Cdc20*), and C7 by canonical DZ markers (*Gcsam*,
167 *Aicda*, *Cxcr4*, and *Foxo1*). Lastly, C4 cells showed an intermediate phenotype between LZ and
168 DZ based on their expression of positive-selection and early proliferation markers *Cd40*, *C1qbp*,
169 *Mybbp1a*, *Myc*, *Mtor*, *Mif*, *Bcl2a1b*, and SHM and CSR marker *Ung* (35, 37–39), which is also a
170 downstream target of Myc (40). Additionally, based on the high expression of Myc- and mTORC1-
171 targeted genes (**fig. S2A**), the majority of C4 cells are likely positively selected B cells. These
172 clusters are consistent with phenotypes observed in prior studies of mouse and human GC B cells
173 (36, 41–43) (**fig. S2B-D**).

174 To further validate our clustering, we performed RNA velocity analysis (**Fig. 2E**). The
175 velocity vector fields showed a bifurcation among LZ cells (C3) towards pre-MBC (C2) or
176 transitioning back to the DZ (C4, C5) (**Fig. 2E**). Cyclical cell division in the DZ was well-reflected
177 by vector fields moving from C5 to C6 to C7 (**Fig. 2E**). The pseudotemporal ordering of antigen-
178 binding GC B cells based on the latent time calculated from RNA velocity revealed a continuum
179 of differentiation trajectory from LZ (C3) or G1 DZ (C7) to cell division in the DZ (C5, C6) and
180 eventual exit as plasmablasts (C1) or pre-MBCs (C2) (**Fig. 2F**, **fig. S2E**). The LZ/DZ intermediate
181 cells (C4) spanned a wide range of latent time, with the majority having high latent time,
182 implicating longer residence in the GC and supporting the posit of positively selected B cells. In
183 summary, our transcriptional profiling is consistent with the current understanding of GC reactions
184 (3, 35).

185

186

187 **Alum-pSer/SMNP combination adjuvant elicits an enrichment of S-phase GC B cells**

188 GC B cells recovered from SMNP- and alum-pSer/SMNP-immunized mice showed substantially
189 greater proportions of B cells in S phase (C5, **Fig. 2G-H, fig. S2F**). Such an observation is of
190 interest because the enrichment of S-phase B cells has been correlated with the strength of positive
191 selection occurring in the LZ (44, 45). Positively selected LZ B cells express *Myc* and mTOR
192 complex 1 (mTORC1, consisting of *Mtor*, *Rptor*, *Akt1s1*, and *Deptor*) as they enter S phase and
193 migrate back to the DZ, and *Myc* expression level is directly proportional to the selection signal
194 strength (3, 44–47). Notably, we observed higher expression of *Myc* and mTORC1 in positively
195 selected LZ/DZ intermediate cells (C4) from SMNP- and alum-pSer/SMNP-immunized mice
196 compared to alum-pSer alone (**Fig. 2I, fig. S2G**); the target genes of *Myc* and mTORC1 (**Data S1**,
197 retrieved from (48, 49) were also significantly upregulated in alum-pSer/SMNP and trended higher
198 in SMNP ($p_{Myc\text{-target}}=0.077$ and $p_{mTORC1\text{-target}}=0.058$) compared to alum-pSer (**Fig. 2J, fig. S2G**).
199 B cells that capture more antigens and receive stronger T cell help signals in the LZ can undergo
200 more proliferative cycles in the DZ (44–46). Prolonged activation of E2F family transcription
201 factors was reported to drive this “inertial” cell division in the absence of extrinsic signals (45,
202 50). We found higher expression of activating E2Fs (*E2f1*, *E2f2*, *E2f3*) among positively selected
203 (C4) and S phase (C5) cells from the combination alum-pSer/SMNP group compared to alum-pSer
204 alone (**Fig. 2K, fig. S2G**). Collectively, these results suggest that the combination adjuvant may
205 have enabled antigen-binding GC B cells to capture more antigen, leading to greater positive
206 selection signals and more cycles of cell division in the DZ.

207

208 **Combining alum-pSer slow antigen delivery with SMNP augments both clonal expansion
209 and clonal diversity**

210 We next turned to paired heavy/light chain scBCR-seq to determine how alum-pSer and SMNP
211 adjuvants impacted the repertoire of antigen-binding B cells recruited to the GC. After rigorous
212 quality control, we recovered full-length heavy chain sequences from 2,286 MD39-binding B cells,
213 full-length light chain sequences from 5,931 MD39-binding B cells, and paired BCR sequences
214 from 1,460 MD39-binding B cells; on average, we recovered BCR sequences from 7, 9, and 14
215 mice immunized with alum-pSer, SMNP, and alum-pSer/SMNP, respectively (**fig. S3A**).
216 Recovered BCRs were distributed across phenotypic clusters (**fig. S3B**), and B cells from
217 expanded clones were enriched in S-phase (**fig. S3C**). Greater proportions of GC B cells from
218 SMNP and alum-pSer/SMNP immunized mice class switched to IgG isotypes, a finding consistent
219 with ELISA analysis of serum Ig isotypes assessed at day 28 (**fig. S3D-E**).

220 A first striking observation was that clone sizes from mice immunized with the
221 combination alum-pSer/SMNP vaccine were much larger than either individual adjuvant group,
222 with twenty-seven clones comprised of 10 or more cells (**Fig. 3A**). By contrast, SMNP
223 immunization elicited only six clones with more than 10 cells and alum-pSer primed very low
224 levels of clonal expansion (**Fig. 3A**). As another measure of clonal expansion, we quantified clonal
225 evenness for cells recovered from individual mice using Pielou's evenness score (J) (51). This
226 analysis revealed a significantly lower J score for the combination and SMNP compared to alum-
227 pSer (**Fig. 3B**). Lower clonal evenness corroborates greater clonal expansion due to the expansion
228 of a sub-portion of the overall clones (52). We next examined the number of unique clones in the
229 GC and observed that substantially more clones were primed by the alum-pSer/SMNP compared
230 to alum-pSer alone (9.8-fold more) or SMNP (2.5-fold more), and SMNP elicited 4.0-fold more

231 clones than the alum-pSer group (**Fig. 3C**). Plotting recovered clonotypes from each mouse ranked
232 by their clone sizes revealed that alum-pSer/SMNP combination vaccine simultaneously
233 augmented clonal expansion of individual clones and recruited a greater quantity of unique clones
234 into the GC reaction (**Fig. 3D**). Thus, the combination adjuvant immunization both recruited more
235 clones to the GC and triggered greater clonal expansion.

236

237 Alum-pSer/SMNP vaccination enhances GC repertoire diversity

238 Many bnAbs for HIV have extensive SHM and require specific heavy and light chain V genes (8–
239 11, 13, 14). Vaccines capable of recruiting diverse B cell clones would be advantageous to increase
240 the likelihood of priming rare precursors capable of evolving toward broad neutralization (10, 11,
241 13, 16, 18). We thus sought to evaluate the BCR heavy and light chain SHM and pairing diversity.

242 We first counted synonymous and replacement nucleotide mutations in the recovered GC
243 BCRs based on inferred germline sequences and found comparable heavy and light chain mutation
244 counts across the vaccine groups (**Fig. 3E**, **fig. S3F**), consistent with prior work suggesting that
245 degrees of SHM are influenced more by elapsed time post-immunization rather than vaccine
246 formulation (16, 17, 43). While the SMNP group showed a statistically significant increase in
247 heavy chain SHM counts over the alum-pSer/SMNP group, the effect size was one nucleotide.

248 To quantify heavy and light chain pairing diversity, we collapsed cells into their respective
249 clones and aggregated clones by V gene pairs. We calculated the Shannon diversity index (H) for
250 each group (53), where each unique V gene pair represents one species and the number of clones
251 using the pair represents the abundance of that species. The calculation showed increasing
252 diversity scores in the order of alum-pSer/SMNP > SMNP > alum-pSer (**fig. S3G-I**). The same
253 calculation was done for each mouse, and the same hierarchy was observed, with the combination
254 adjuvant showing significantly greater BCR pairing diversity than alum-pSer alone and a trend of
255 greater diversity than SMNP alone ($p=0.073$, **Fig. 3F**). To determine whether this result reflected
256 the larger size of GCs primed by the combination adjuvant or an emergent property due to the
257 alum-pSer/SMNP formulation, we performed sub-sampling analyses on alum-pSer/SMNP (where
258 1222 paired BCR sequences and 303 unique clones were recovered, respectively) and SMNP (225
259 paired BCR sequences recovered, 104 clones) groups by random sampling either 200 BCRs or 100
260 clones from each group, calculating pairing diversity scores for each mouse, performing a two-
261 tailed t-test, and repeating the process 10,000 times to generate distributions of p-values (**fig. S3J**).
262 Neither analysis showed statistical significance, suggesting that the increasing trend of BCR
263 pairing diversity was primarily correlated with overall GC size.

264 We observed overlaps among the most frequently used BCR pairs across the vaccine
265 groups (e.g., Ighv3-2—Igkv3-2, Ighv12-1-1—Igkv3-5, and Ighv15-2—Igkv3-2, **Fig. 3G**), which
266 motivated us to perform an analysis for public clones. Based on their use of (1) the same V and J
267 genes, (2) the same HCDR3 length, and (3) a similarity threshold of their HCDR3 amino acid
268 sequences, we grouped B cell clones into meta-clonotypes across mice and vaccine formulations.
269 We defined “public clones” as meta-clonotypes encompassing clones from more than one mouse
270 and the rest as “private clones” (**Fig. 3H-I**). This analysis revealed that 4%, 40%, and 21% clones
271 from alum-pSer, SMNP, and alum-pSer/SMNP were grouped into public clones, respectively (**Fig.**
272 **3J**). Among the top 20 public clones, the largest public clone enclosed B cells from all three
273 groups, and 4 public clones from SMNP and alum-pSer/SMNP (**Fig. 3I**). In total, thirty-nine public
274 clones were observed uniquely from the alum-pSer/SMNP group, 2.1-times more than SMNP-

275 unique public clones, suggesting that mice immunized with alum-pSer/SMNP developed more
276 diverse BCR features which were positively selected for recognizing MD39 (**Fig. 3H**).

277 To gauge meta-clonal diversity, we calculated the Shannon diversity index (H) for each
278 vaccine formulation, in which the abundance of each species (unique meta-clonotype) was the
279 amount of enclosed private clones from each formulation (private clones were counted as meta-
280 clonotypes with an abundance of 1). The alum-pSer/SMNP group exhibited the greatest meta-
281 clonal diversity ($H = 6.24$), followed by SMNP ($H = 4.75$) and alum-pSer ($H = 3.22$) (**Fig. 3J**).
282 Altogether, we found that mice vaccinated with alum-pSer/SMNP induced GCs with greater
283 numbers of unique private and public clones. These results suggest that the repertoire of BCRs
284 recruited to GCs following alum-pSer/SMNP immunization is more diverse.
285

286 **Combining alum-anchored immunogens with SMNP promotes trafficking of antigen to 287 lymph node follicles**

288 The scRNA-seq and scBCR-seq analyses showed that combining alum-pSer and SMNP adjuvants
289 increased GC B cell clonal expansion, repertoire diversity, total number of B cell clones recruited
290 to the GC, and increased the proportion of B cells cycling in the DZ – a surprising breadth of effects
291 on the GC response. We thus next sought to investigate potential mechanisms underlying these
292 effects of alum-pSer/SMNP immunization. The observation of S-phase enrichment in alum-
293 pSer/SMNP GC B cells inspired a hypothesis based on our prior findings: heavily glycosylated
294 antigens like HIV Env trimers, when displayed on the surface of nanoparticles, trigger complement
295 deposition *in vivo* via the lectin pathway, resulting in complement-dependent trafficking of the
296 particles to FDCs (54, 55). We hypothesized that alum particles bearing many pSer-anchored
297 trimers could trigger a similar process for trafficking the antigen to FDCs. In parallel, we also
298 previously showed that SMNP triggers rapid depletion of subcapsular sinus macrophages and
299 increased antigen accumulation in dLN (25). These two complementary mechanisms of action
300 may be synergistic in shepherding more MD39 antigen into the follicles and onto the FDC network,
301 which might explain the enrichment of S-phase GC B cells observed in the scRNAseq analysis,
302 because greater antigen uptake is correlated with more cycles of cell division in the DZ (44) (**Fig.**
303 **2G-H, fig. S3C**).

304 Motivated by these ideas, we evaluated the localization of fluorescently labeled MD39
305 trimer in dLN following vaccination with alum-pSer and SMNP. We chose to focus on comparing
306 antigen trafficking of alum-pSer vs. alum-pSer/SMNP because we had previously shown that
307 immunization with Env trimers and SMNP alone does not lead to significant antigen accumulation
308 on FDCs in a primary immunization (16, 56, 57). As a control, we also assessed antigen
309 biodistribution in LNs for SMNP and alum mixed with MD39-Ser₄, a trimer conjugated with a
310 non-phosphorylated serine tag that cannot undergo ligand exchange binding to the alum particles.
311 Mice were immunized with these 3 different vaccines, and inguinal dLN were isolated at varying
312 time points for histological imaging. Following immunization with either alum/MD39-pSer₄ or
313 MD39-Ser₄ combined with both alum and SMNP, minimal antigen accumulation on the FDC
314 network (or at other locations in the LN) was observed at any examined time point (**Fig. 4A-B**).
315 By contrast, when MD39 was bound to alum via a phosphoserine linker and combined with SMNP,
316 substantial antigen accumulation was detected on LN FDCs beginning at day 14, and persisted
317 through day 35 (**Fig. 4C**). Higher magnification imaging showed that this antigen signal
318 colocalized with FDC dendrites (**Fig. 4D**). Quantification of the FDC-localized antigen signal from
319 multiple follicles of multiple LNs over time showed that following alum-pSer/SMNP

320 immunization, antigen accumulation rose sharply between day 7 and day 14, was maintained
321 through day 21, and then slowly decayed thereafter (**Fig. 4E**). This analysis revealed that the
322 combination adjuvant vaccination elicited at least 15-fold greater antigen accumulation on FDCs
323 compared to immunization with alum/MD39-pSer₄ alone. To investigate the mechanistic basis of
324 antigen accumulation on FDCs following alum-pSer/SMNP immunization, we evaluated the
325 localization of fluorescently labeled MD39 trimer in dLNs of mice lacking the C3 component of
326 the complement system (C3 KO) (**Fig. 4F-G**). Strikingly, we observed a substantial reduction in
327 antigen colocalization with FDCs in C3 KO mice compared to wild type C57BL/6 mice,
328 suggesting that the trafficking of antigen to the FDCs following alum-pSer/SMNP immunization
329 is complement-dependent.

330

331 **Env trimer antigen delivered to follicles via combined alum-pSer/SMNP vaccination is**
332 **retained in a highly intact state on FDCs**

333 Antigen localizing to the sinuses and interfollicular regions of the LN undergoes rapid degradation
334 over the first few days post-immunization, while antigens captured on FDCs can be retained in a
335 highly intact state over time due to spatially compartmentalized protease activity in LNs (57). To
336 assess potential degradation of the MD39 trimer *in vivo* following combination alum-pSer/SMNP
337 immunization, we applied a fluorescence resonance energy transfer (FRET)-based approach we
338 previously developed to track antigen integrity in LNs (57). MD39 antigen was labeled with ~6
339 total dyes per trimer (~3 Cy3 donor and ~3 Cy5 acceptor dyes) for FRET imaging. When the
340 antigen undergoes proteolytic degradation, the donor and acceptor dyes become separated, leading
341 to reduced FRET signals proportional to the degree of degradation (**fig. S4A**) (57).

342 We first confirmed that this degree of dye labeling did not significantly alter the alum
343 binding behavior or antigenicity profile of the trimer (**fig. S4B-C**). We next tested whether the
344 binding of dye-labeled MD39-pSer₄ trimer to alum affected the measurement of intermolecular
345 FRET, using an acceptor photobleaching approach to measure energy transfer. We imaged FRET
346 dye-labeled free MD39 or alum-anchored MD39-pSer₄ adsorbed on glass coverslips and observed
347 an enhancement in donor emission following acceptor photobleaching indicative of FRET (**fig.**
348 **S4D-E**). The histograms of FRET efficiencies measured pixel by pixel for free vs. alum-bound
349 trimer overlapped, indicating no significant impact of alum binding on the FRET signal (**fig. S4F**).
350 FRET was only observed when antigens were labeled with both Cy3 and Cy5 on the same trimer,
351 and no intermolecular FRET was observed when Cy3-labeled MD39-pSer₄ trimers were co-loaded
352 with Cy5-labeled MD39-pSer₄ on alum particles, or when alum particles loaded with Cy3-labeled
353 MD39-pSer₄ were mixed with alum particles carrying Cy5-labeled MD39-pSer₄ (**fig. S4G**). These
354 controls indicate that FRET detected *in vivo* should reflect intact trimeric antigen and not
355 intermolecular FRET between adjacent trimers loaded on alum or bound to FDCs. In addition, the
356 FRET efficiency was not influenced by adding Cy3/Cy5-specific antibodies to the labeled trimer
357 (**fig. S4H**), suggesting that potential anti-dye antibody responses which could theoretically be
358 elicited by dye-labeled MD39 immunization would not alter the FRET efficiency readout. As
359 expected based on our previous work, a decline in FRET efficiency was observed following the
360 incubation of FRET-labeled, alum-bound trimer with the promiscuous protease trypsin (**fig. S5A-**
361 **B**). This correlated with a reduction in the binding of antibodies targeting the interface/fusion
362 peptide, V3 epitopes, and CD4 binding site on the trimer as measured by ELISA (**fig. S5C**).
363 Overall, these data indicated that FRET-based imaging is sensitive to detect changes in the
364 structural integrity of the trimer.

Having established the ability of the FRET assay to track MD39 trimer integrity when bound to alum, we next evaluated trimer stability in the context of alum-pSer and SMNP immunizations *in vivo*. Given that alum-bound trimer is expected to slowly clear from the injection site over time, we first investigated antigen stability at the injection site. To address this, mice were immunized subcutaneously with FRET dye-labeled MD39-Ser₄ or MD39-pSer₄ mixed with alum and SMNP adjuvants, and injection site tissues were isolated at varying time points post-immunization. While only low levels of MD39-Ser₄ remained at the injection site by day 7 (**Fig. 5A**), alum-anchored MD39-pSer₄ was still detectable at high levels at this time point and remained detectable at the injection site through day 21 (**Fig. 5A**), consistent with prior whole animal fluorescence imaging studies (20). Acceptor photobleaching FRET was used to determine the fraction of intact antigen at the injection site for each condition and timepoint, revealing that while there was a decline in antigen stability over time, ~50% of alum-anchored MD39-pSer₄ was still intact at the injection site 21 days after immunization (**Fig. 5B-C**).

In parallel, we imaged antigen accumulated on the FDC network in draining inguinal lymph nodes. Strikingly, a majority of antigen that accumulated on the FDCs following alum-pSer/SMNP immunization was non-degraded and remained intact through day 28 (**Fig. 5D-G**). Altogether, these data indicate that unlike alum-pSer or SMNP adjuvants individually, the combination alum-pSer/SMNP immunization leads to pronounced antigen targeting to FDCs over time, and this antigen is retained in a highly intact state for at least one month post-immunization, all factors that would be expected to help augment recruitment of trimer-specific B cells to the GC response.

386

387 DISCUSSION

388

Slow-delivery vaccine approaches promote early immune complex formation and sustained antigen delivery to B cells, which has been shown to increase the diversity of recruited clones and correlated with enhanced neutralization breadth (15–17). On the other hand, particulate display of antigens is conducive to BCR crosslinking and B cell activation, which has been shown to facilitate the activation and recruitment of diverse precursors B cells, restrict access to base-proximal epitopes, and cultivate the maturation of low-affinity precursors (54, 56, 58, 59). These distinct (and we hypothesized, complementary) mechanisms of action underlying slow delivery and particulate antigen formulations inspired our initial studies examining the alum-pSer/SMNP adjuvant combination. Here, we showed that this combination adjuvant vaccine, which incorporates slow-delivery, multivalent anchoring of immunogens onto alum, and a potent adjuvant, enhanced multiple facets of the humoral immune response including greater GC B cell, Tfh cell, and serum IgG antibody responses. Although mice are generally unable to elicit bnAb-lineage B cell responses due to their short CDR3 domains (60), we found that this combination adjuvant strategy recruited a more clonally expanded and diverse B cell response and resulted in a repertoire with broader BCR characteristics to recognize the MD39 trimer immunogen—all features expected in humans to promote priming of rare precursor B cells that are needed for bnAb responses against HIV and other infectious diseases.

One important consideration for vaccine slow delivery approaches is the possibility of antigen degradation over time following administration, either at the injection site or en route to draining lymph nodes. Despite the promise of the alum-pSer approach to promote sustained

409 delivery of antigen *in vivo*, when exposed to physiological conditions, including proteases and
410 thermal stress for extended periods of time, antigen breakdown could occur that could influence B
411 cell competition and immunodominance, diverting responses toward vaccine-irrelevant
412 breakdown product epitopes (61). Previous studies have pointed to both positive and negative
413 impacts of alum on antigen integrity and stability: adsorption of proteins onto alum has been
414 reported to result in protein unfolding, potentially due to the nature of the protein-alum interactions
415 or the duration of the binding (62–64), while others point to a stabilizing role for antigen adsorption
416 on alum for antigen integrity, particularly when exposed to thermal stress (65). Extensive efforts
417 have sought to stabilize HIV Env immunogens through molecular engineering (66), and we
418 hypothesized that alum-anchoring of pSer-Env trimers might partially shield immunogens from
419 protease-mediated degradation. Using a FRET imaging-based approach to track antigen integrity
420 over time, we found that a majority of alum-bound pSer-trimer remained intact for at least 28 days
421 post-injection (**Fig. 5G**). Since our approach utilizes a phosphoserine peptide tag to mediate
422 antigen-alum ligand exchange interactions, it is possible this alum-pSer platform may be less
423 susceptible to antigen-specific stability phenomena observed in the literature.

424 Another important facet of vaccine design is the ability of antigens to traffic to the FDC
425 network. Previous studies have demonstrated that antigen particles decorated with complement
426 (either due to innate immune recognition or immune complex formation (67–69)), efficiently
427 accumulate on FDCs, leading to enhanced GC and serum antibody responses (54, 56). Antigens
428 captured by FDCs shape the B cell response, as FDCs present antigens to B cells in the follicle
429 where activated B cells undergo proliferation and SHM to generate high-affinity antibodies (69,
430 70). Notably, soluble HIV trimer immunogens delivered as bolus injections predominantly localize
431 in interfollicular regions via SIGN-R1⁺ lymph node macrophages, which capture the trimer from
432 the afferent lymph, rather than trafficking to FDCs (54, 71). Being able to deliver antigens onto
433 the FDC network is of interest because FDCs can recycle and protect antigens captured on their
434 dendrites (67) and the follicles are sanctuary sites with low protease activity in lymph nodes where
435 antigens are protected from proteolytic degradation (57). It is known that protein nanoparticles or
436 immune complexes decorated with complement are shuttled to FDCs in a complement- and
437 complement receptor-dependent manner, mediated by noncognate B cells picking up the
438 complement-decorated antigen and transferring it to FDCs (54, 68, 72–74). In the present case,
439 there are at least 3 possible pathways for alum/pSer-trimer particles to trigger complement
440 deposition: (i) early antibody responses elicited over the first 1–2 weeks could promote the
441 formation of immune complexes as alum/pSer-trimer complexes slowly drain from the remaining
442 injection site depot to the dLN, similar to effects observed with repeat-injection immunizations
443 (15, 16); (ii) the alum particles may directly activate complement (75, 76) leading to C3 decoration
444 of the alum/pSer-trimer complexes; or (iii) complement deposition could be triggered by mannose
445 binding lectin recognition of trimer-decorated alum particles (54). While we show here FDC
446 homing of antigen following the combination adjuvant vaccination is dependent on complement,
447 further dissecting whether one or more of these pathways governs this response remains an open
448 question for future work. SMNP is expected to amplify this antigen delivery process by causing
449 early depletion of subcapsular sinus macrophages that limit antigen entry into the dLN.

450 In conclusion, these studies demonstrate how combining slow antigen delivery via
451 immunogen anchoring on alum with a potent saponin/TLR agonist adjuvant can alter antigen
452 biodistribution in lymph nodes, leading to a sustained buildup of intact antigen captured in B cell
453 follicles. This alteration in antigen delivery correlates with substantial changes in the composition
454 of the germinal center response triggered by the combination of these two adjuvants: including

455 recruitment of a significantly more diverse set of B cell clones to the GC, which also undergo
456 greater clonal expansion compared to vaccines using either adjuvant alone. More broadly, this
457 work reinforces the idea that combining advancements in vaccine delivery with developments in
458 adjuvant technologies can enable the induction of distinctly different immune responses to
459 immunization via novel mechanisms of action.

460 **MATERIALS AND METHODS**

461 Study design

462 The objective of these studies was to investigate the mechanism by which the combination of
463 alum-anchored pSer-modified HIV Env immunogens with SMNP adjuvant elicits significantly
464 improved humoral immune responses, as a clinically translatable approach to promote slow
465 delivery of vaccine following a single injection. Mice were immunized and subsequent humoral
466 immune responses (germinal center responses, T follicular helper responses, and serum antibody
467 responses) were assessed by flow cytometry, ELISA, and single-cell RNA sequencing. Antigen
468 trafficking studies were completed using fluorescently labeled antigens and imaged by confocal
469 microscopy using acceptor photobleaching to track antigen integrity via FRET. This acceptor
470 photobleaching method avoids donor and acceptor crosstalk and is not influenced by dye
471 concentrations or ratios. Group sizes were selected based on effect sizes seen in prior studies.

472 Antigen production and pSer conjugation

473 MD39 immunogens with or without a free C-terminal cysteine and containing a positively charged,
474 non-polyhistidine amino acid sequence (Lys-Lys-Lys) at the C-terminus of the trimer with or
475 without a filled glycan hole at residues N241 and N289 (20, 77, 78) were synthesized as described
476 previously (27, 79). Briefly, genes encoding MD39 HIV Env gp140 were cloned into pHlsec by
477 Genscript and co-transfected with human furin in a pcDNA3.1 plasmid using a 2:1 trimer:furin
478 DNA ratio with polyethylenimine into FreeStyle 293-F cells (ThermoFisher) and incubated for 6
479 days. The cultures were centrifuged and the supernatants containing MD39 were harvested and
480 purified using a HisTrap HP column (Cytiva Life Sciences) with an AKTA FPLC system (Cytiva
481 Life Sciences) for immunogens expressed with a polyhistidine linker and a 2G12 immunoaffinity
482 column for MD39 immunogens without a polyhistidine linker. The immunogens were further
483 purified by size-exclusion chromatography with an S200 Increase column (Cytiva Life Sciences)
484 in TBS at flow rate of 0.5 mL/min. Size exclusion chromatography multi-angle light-scattering
485 (SECMALS, DAWN HELEOS II and Optilab T-rEX Wyatt Technology) was then used to confirm
486 the trimer molecular weights.

487 Immunogens expressed with a free terminal cysteine were reduced at 1 mg/mL with 10
488 molar equivalents of tris(2-carboxyethyl)phosphine (TCEP, ThermoFisher) in TBS and incubated
489 at 25°C for 10 minutes. TCEP was subsequently removed from the reduced protein solution using
490 Amicon Ultra Centrifugal Filters (10 kDa MWCO, Millipore Sigma) in tris-buffered saline (TBS,
491 Sigma Aldrich), and 1 mg/mL reduced antigen was reacted with 5 molar equivalents of Ser₄-
492 maleimide or pSer₄-maleimide linkers for 16 hours at 4°C in TBS (pH 7.2-7.4). Free peptide linker
493 was subsequently removed using 10 kDa MWCO centrifugal filters in TBS, and pSer-antigen was
494 buffer exchanged to PBS.

495 pSer₄-conjugated cytochrome C used for antigenicity profiling of immunogens was
496 prepared as described (18), using cytochrome C from *Saccharomyces cerevisiae* (Sigma Aldrich).
497 The number of pSer residues conjugated to the antigen was assessed using the Malachite Green
498 Phosphoprotein Phosphate Estimation Assay Kit (Thermo Scientific) against a standard curve of
499 pSer-maleimide linker. Signal from pSer-antigen was compared to the background from an
500 unconjugated antigen control.

501 Animals and immunizations

502 Experiments and handling of mice were conducted under federal, state, and local guidelines under
503 an Institutional Animal Care and Use Committee (IACUC)-approved protocol. Female 6-8-week-
504 old BALB/c, C57BL/6, and C3 KO mice were purchased from the Jackson Laboratory (stock no.
505 000651, 000664, and 029661, respectively). Immunizations for sequencing studies were prepared
506 by mixing 5 µg of antigen with a glycan hole at residues N241 and N289 and 50 µg of alum in 100
507 µL sterile tris-buffered saline (TBS, Sigma Aldrich) per mouse. Immunizations for histology and
508 FRET studies were prepared by mixing 10 µg of antigen with a filled glycan hole at residues N241
509 and N289 and 100 µg of alum in 100 µL sterile tris-buffered saline (TBS, Sigma Aldrich) per
510 mouse. Antigen was loaded onto alum for 30 minutes on a tube rotator prior to immunization. For
511 alum-pSer/SMNP combination vaccines, antigen was first loaded onto alum for 30 minutes on a
512 rotator, after which 5 µg of SMNP was added and incubated with antigen-alum formulations for
513 30 minutes prior to immunization. This dose of SMNP corresponds to 5 µg of Quil-A saponin and
514 0.5 µg MPLA. For sequencing studies, BALB/c mice were immunized subcutaneously at the tail
515 base with 50 µL on each side of the tail base with one of three formulations: alum-pSer (5 µg
516 MD39-pSer₄ and 50 µg alum total), SMNP (5 µg MD39 mixed with 5 µg SMNP) or alum-
517 pSer/SMNP (5 µg MD39-pSer₄ combined with 50 µg alum and 5 µg SMNP).

518 scRNA-seq study design, processing, and analysis

519 The inguinal LNs of vaccinated mice (n=14 animals/group) were isolated 14 days post-
520 immunization. LNs were mashed and passed through a 70um filter to obtain single-cell
521 suspensions. Cells were stained for viability (ThermoFisher Live/Dead FixableAqua) and with
522 antibodies against CD3e (BV711, BioLegend, 145-2C11clone), CD19 (APC, BioLegend, 6D5
523 clone), B220 (PE-Cy7, BioLegend RA3-6B2 clone), CD38 (FITC, BioLegend 90 clone), GL7
524 (PerCP-Cy5.5, BioLegend GL7 clone), and labeled with TotalSeq-B cell hashing antibodies
525 (BioLegend). Antigen-specific staining was completed using biotinylated MD39 conjugated to
526 streptavidin-BV421 (BioLegend) and streptavidin-PE (BioLegend). Antigen double-positive GC
527 B cells were sorted on a BD FACS Aria (BD Biosciences) cell sorter and processed immediately
528 following the SeqWell protocol (**Table S1**) (28, 29). scRNA-seq libraries were sequenced by
529 Illumina NovaSeq and aligned to the mm10 reference genome using the STARSolo pipeline
530 (version 2.4.0) (80). The gene expression count matrix and cell hashing sequence reads were
531 processed and analyzed using Seurat (v4.1.0), CITE-seq-Count v1.4.2, Scanpy, and scVelo (81–
532 84) (for detailed procedures, see Supplementary Materials and Methods).

533 Myc- and mTORC1-target genes (**Data S1**) were retrieved from the literature (45, 48, 49)
534 and their gene set module scores were calculated using the AddModuleScore() function in Seurat
535 (81). Data from Mathew et al., King et al., and Holmes et al. were obtained from
536 ArrayExpress with accession numbers E-MTAB-9478, E-MTAB-9005, and from Gene
537 Expression Omnibus database GSE139891, respectively (41–43). Differentially expressed genes
538 of relevant clusters from these studies were mapped onto our scRNA-seq data using the
539 AddModuleScore() function (81).

540 scBCR-seq library generation, sequencing, processing, and analysis

541 The scBCR-seq library was prepared as described previously (30). In brief, the immunoglobulin
542 (Ig) transcripts were enriched and amplified from the 3'-barcoded cDNA (**Table S2**). A set of V-
543 gene primers (modified from Tillers et al. (85)) (**Table S3**), were used to further enrich
544 immunoglobulin transcripts before sequencing (**Table S4-S5**). BCR sequence reads were
545 processed with pRESTO (v0.5.13), Change-O (v0.4.6), UMI-Tools, and IgBlast (v1.14.0) (86–89)

546 to reconstruct and annotate full-length BCR sequences that match corresponding single-cell
547 transcriptomes (for detailed procedures, see Supplementary Materials and Methods).

548 Clonally related sequences were identified using the DefineClones.py function (Change-O
549 v0.4.6) with a 90% CDR3 nucleotide similarity threshold determined by distToNearst() function
550 from the Shazam package (87). Germline sequences were inferred using the CreateGermline.py
551 function (Change-O v0.4.6) (87). Meta-clonotypes were identified based on the shared V gene, J
552 gene, CDR3 junction length, and 94% CDR3 amino acid similarity threshold determined by
553 distToNearst() function. Clone sizes, or the number of cells per clone, were calculated using the
554 countClones() function (alakazam v1.2.1). Clonal evenness was quantified for each mouse by
555 Pielou's evenness index (J) (51). It was calculated as the Shannon Diversity Index (H) divided by
556 the natural log of the total number of clones in each mouse (53). A J value of 1 means that all the
557 clones in the mouse have the same number of cells.

558 SHM counts were aggregated using the observedMutations() (Shazam v1.1.2) function
559 (87). The Circos plots were generated using the “circlize” package (90). BCR pairing diversity
560 was calculated in the following steps: first, cells were collapsed into their respective clones. If a
561 clone matched to more than one light chain V gene, the light chain V gene with the most cells in
562 the clone was designated for the clone. Second, clones were aggregated into unique BCR pairs and
563 the number of clones using a unique BCR pair was counted. Lastly, Shannon's Diversity Index
564 was calculated for each group, whereby each unique V gene pair was the “species” and the number
565 of clones using the pair was the “abundance” for the “species”. The same calculation was also
566 performed at the individual mouse level.

567 Confocal microscopy

568 Imaging was performed on a Leica SP8 confocal microscope using white light and argon lasers
569 with spectral emission filters with a minimum bandwidth of 10 nm. A 25X water-immersion
570 objective was used unless otherwise indicated. Laser and detector settings were kept constant
571 across all imaging timepoints for each antigen. FRET efficiency was calculated as previously
572 described (57). Images were processed and analyzed in ImageJ (version 2.1.0/1.53c).

573 Statistical Analysis

574 For sequencing analysis, statistical analysis was performed in the R software version 4.3.0. The
575 specific statistical tests are indicated in the figure legends. All other data were plotted and all
576 statistical analyses were performed using GraphPad Prism 9 software (La Jolla, CA). All graphs
577 display mean values, and the error bars represent the standard deviation unless otherwise specified.
578 No samples or animals were excluded from the analyses. Statistical comparison was performed
579 using a one-way ANOVA followed by Tukey's post-hoc test for single timepoint data with three
580 or more groups and two-way ANOVA followed by Tukey's post-hoc test for multi-timepoint
581 longitudinal data unless otherwise indicated. Data were considered statistically significant if the
582 p-value was less than 0.05.

583 **List of Supplementary Materials**

584 Supplementary Materials and Methods

585 Fig S1 to S5

586 Data S1

587 Tables S1 to S5

588 **References and Notes**

589

- 590 1. A. J. Pollard, E. M. Blijker, A guide to vaccinology: from basic principles to new
591 developments. *Nat. Rev. Immunol.* **21**, 83–100 (2021).
- 592 2. I. J. Amanna, M. K. Slifka, Contributions of humoral and cellular immunity to vaccine-
593 induced protection in humans. *Virology* **411**, 206–215 (2011).
- 594 3. G. D. Victora, M. C. Nussenzweig, Germinal Centers. [https://doi.org/10.1146/annurev-
595 immunol-020711-075032](https://doi.org/10.1146/annurev-immunol-020711-075032) **30**, 429–457 (2012).
- 596 4. Y. Z. Cohen, R. Dolin, Novel HIV vaccine strategies: overview and perspective. *Ther. Adv.
597 Vaccines* **1**, 99–112 (2013).
- 598 5. J. M. Steichen, Y.-C. Lin, C. Havenar-Daughton, S. Pecetta, G. Ozorowski, J. R. Willis, L.
599 Toy, D. Sok, A. Liguori, S. Kratochvil, J. L. Torres, O. Kalyuzhniiy, E. Melzi, D. W. Kulp, S.
600 Raemisch, X. Hu, S. M. Bernard, E. Georges, N. Phelps, Y. Adachi, M. Kubitz, E. Landais, J.
601 Umotoy, A. Robinson, B. Briney, I. A. Wilson, D. R. Burton, A. B. Ward, S. Crotty, F. D.
602 Batista, W. R. Schief, A generalized HIV vaccine design strategy for priming of broadly
603 neutralizing antibody responses. *Science* **366** (2019), doi:10.1126/science.aax4380.
- 604 6. S. Su, W. Li, S. Jiang, Developing pan-β-coronavirus vaccines against emerging SARS-CoV-2
605 variants of concern. *Trends Immunol.* **43**, 170–172 (2022).
- 606 7. L. K. Schrager, J. Vekemens, N. Drager, D. M. Lewinsohn, O. F. Olesen, The status of
607 tuberculosis vaccine development. *Lancet Infect. Dis.* **20**, e28–e37 (2020).
- 608 8. F. Klein, H. Mouquet, P. Dosenovic, J. F. Scheid, L. Scharf, M. C. Nussenzweig, Antibodies
609 in HIV-1 Vaccine Development and Therapy. *Science* **341**, 1199–1204 (2013).
- 610 9. M. D. Simek, W. Rida, F. H. Priddy, P. Pung, E. Carrow, D. S. Laufer, J. K. Lehrman, M.
611 Boaz, T. Tarragona-Fiol, G. Miilo, J. Birungi, A. Pozniak, D. A. McPhee, O. Manigart, E.
612 Karita, A. Inwoley, W. Jaoko, J. Dehovitz, L.-G. Bekker, P. Pitisuttithum, R. Paris, L. M.
613 Walker, P. Poignard, T. Wrin, P. E. Fast, D. R. Burton, W. C. Koff, Human immunodeficiency
614 virus type 1 elite neutralizers: individuals with broad and potent neutralizing activity identified
615 by using a high-throughput neutralization assay together with an analytical selection algorithm.
616 *J. Virol.* **83**, 7337–48 (2009).
- 617 10. P. D. Kwong, J. R. Mascola, G. J. Nabel, Broadly neutralizing antibodies and the search for
618 an HIV-1 vaccine: the end of the beginning. *Nat. Rev. Immunol.* **13**, 693–701 (2013).
- 619 11. B. F. Haynes, K. Wiehe, P. Borrow, K. O. Saunders, B. Korber, K. Wagh, A. J. McMichael,
620 G. Kelsoe, B. H. Hahn, F. Alt, G. M. Shaw, Strategies for HIV-1 vaccines that induce broadly
621 neutralizing antibodies. *Nature Reviews Immunology* **23**:3 **23**, 142–158 (2022).

- 622 12. B. S. Briney, J. R. Willis, M. D. Hicar, J. W. Thomas, J. E. Crowe, Frequency and genetic
623 characterization of V(DD)J recombinants in the human peripheral blood antibody repertoire.
624 *Immunology* **137**, 56–64 (2012).
- 625 13. N. A. Doria-Rose, C. A. Schramm, J. Gorman, P. L. Moore, J. N. Bhiman, B. J. DeKosky,
626 M. J. Ernandes, I. S. Georgiev, H. J. Kim, M. Pancera, R. P. Staupe, H. R. Alatae-Tran, R. T.
627 Bailer, E. T. Crooks, A. Cupo, A. Druz, N. J. Garrett, K. H. Hoi, R. Kong, M. K. Louder, N. S.
628 Longo, K. McKee, M. Nonyane, S. O'Dell, R. S. Roark, R. S. Rudicell, S. D. Schmidt, D. J.
629 Sheward, C. Soto, C. K. Wibmer, Y. Yang, Z. Zhang, N. C. S. Program, J. C. Mullikin, J. M.
630 Binley, R. W. Sanders, I. A. Wilson, J. P. Moore, A. B. Ward, G. Georgiou, C. Williamson, S. S.
631 A. Karim, L. Morris, P. D. Kwong, L. Shapiro, J. R. Mascola, Developmental pathway for potent
632 V1V2-directed HIV-neutralizing antibodies. *Nature* **509**, 55–62 (2014).
- 633 14. L. M. Walker, S. K. Phogat, P.-Y. Chan-Hui, D. Wagner, P. Phung, J. L. Goss, T. Wrin, M.
634 D. Simek, S. Fling, J. L. Mitcham, J. K. Lehrman, F. H. Priddy, O. A. Olsen, S. M. Frey, P. W.
635 Hammond, P. G. P. Investigators, S. Kaminsky, T. Zamb, M. Moyle, W. C. Koff, P. Poignard, D.
636 R. Burton, Broad and Potent Neutralizing Antibodies from an African Donor Reveal a New HIV-
637 1 Vaccine Target. *Science* **326**, 285–289 (2009).
- 638 15. H. H. Tam, M. B. Melo, M. Kang, J. M. Pelet, V. M. Ruda, M. H. Foley, J. K. Hu, S.
639 Kumari, J. Crampton, A. D. Baldeon, R. W. Sanders, J. P. Moore, S. Crotty, R. Langer, D. G.
640 Anderson, A. K. Chakraborty, D. J. Irvine, Sustained antigen availability during germinal center
641 initiation enhances antibody responses to vaccination. *Proc National Acad Sci* **113**, E6639–
642 E6648 (2016).
- 643 16. K. M. Cirelli, D. G. Carnathan, B. Nogal, J. T. Martin, O. L. Rodriguez, A. A. Upadhyay, C.
644 A. Enemuo, E. H. Gebru, Y. Choe, F. Viviano, C. Nakao, M. G. Pauthner, S. Reiss, C. A.
645 Cottrell, M. L. Smith, R. Bastidas, W. Gibson, A. N. Wolabaugh, M. B. Melo, B. Cossette, V.
646 Kumar, N. B. Patel, T. Tokatlian, S. Menis, D. W. Kulp, D. R. Burton, B. Murrell, W. R. Schief,
647 S. E. Bosinger, A. B. Ward, C. T. Watson, G. Silvestri, D. J. Irvine, S. Crotty, Slow Delivery
648 Immunization Enhances HIV Neutralizing Antibody and Germinal Center Responses via
649 Modulation of Immunodominance. *Cell* **177**, 1153–1171.e28 (2019).
- 650 17. J. H. Lee, H. J. Sutton, C. A. Cottrell, I. Phung, G. Ozorowski, L. M. Sewall, R. Nedellec, C.
651 Nakao, M. Silva, S. T. Richey, J. L. Torre, W. H. Lee, E. Georges, M. Kubitz, S. Hodges, T.
652 Mullen, Y. Adachi, K. M. Cirelli, A. Kaur, C. Allers, M. Fahlberg, B. F. Grasperge, J. P.
653 Dufour, F. Schiro, P. P. Aye, O. Kalyuzhniy, A. Liguori, D. G. Carnathan, G. Silvestri, X. Shen,
654 D. C. Montefiori, R. S. Veazey, A. B. Ward, L. Hangartner, D. R. Burton, D. J. Irvine, W. R.
655 Schief, S. Crotty, Long-primed germinal centres with enduring affinity maturation and clonal
656 migration. *Nature* **2022** *609*:7929 **609**, 998–1004 (2022).
- 657 18. T. J. Moyer, Y. Kato, W. Abraham, J. Y. H. Chang, D. W. Kulp, N. Watson, H. L. Turner, S.
658 Menis, R. K. Abbott, J. N. Bhiman, M. B. Melo, H. A. Simon, S. H.-D. la Mata, S. Liang, G.
659 Seumois, Y. Agarwal, N. Li, D. R. Burton, A. B. Ward, W. R. Schief, S. Crotty, D. J. Irvine,
660 Engineered immunogen binding to alum adjuvant enhances humoral immunity. *Nature Medicine*
661 **26**, 430–440 (2020).

- 662 19. K. A. Rodrigues, S. A. Rodriguez-Aponte, N. C. Dalvie, J. H. Lee, W. Abraham, D. G.
663 Carnathan, L. E. Jimenez, J. T. Ngo, J. Y. H. Chang, Z. Zhang, J. Yu, A. Chang, C. Nakao, B.
664 Goodwin, C. A. Naranjo, L. Zhang, M. Silva, D. H. Barouch, G. Silvestri, S. Crotty, J. C. Love,
665 D. J. Irvine, Phosphate-mediated coanchoring of RBD immunogens and molecular adjuvants to
666 alum potentiates humoral immunity against SARS-CoV-2. *Science Advances* **7**, 6538 (2021).
- 667 20. K. A. Rodrigues, C. A. Cottrell, J. M. Steichen, B. Groschel, W. Abraham, H. Suh, Y.
668 Agarwal, K. Ni, J. Y. H. Chang, P. Yousefpour, M. B. Melo, W. R. Schief, D. J. Irvine,
669 Optimization of an alum-anchored clinical HIV vaccine candidate. *npj Vaccines* **8**, 117 (2023).
- 670 21. B. Pulendran, P. S. Arunachalam, D. T. O'Hagan, Emerging concepts in the science of
671 vaccine adjuvants. *Nat. Rev. Drug Discov.* **20**, 454–475 (2021).
- 672 22. G. D. Giudice, R. Rappuoli, A. M. Didierlaurent, Correlates of adjuvanticity: A review on
673 adjuvants in licensed vaccines. *Semin. Immunol.* **39**, 14–21 (2018).
- 674 23. A. Didierlaurent, A. Berger, T. Heineman, V. Henderickx, F. T. D. Silva, J. Vekemans, G.
675 Voss, N. Garcon, in (Elsevier, 2017), pp. 265–285.
- 676 24. P. T. Heath, E. P. Galiza, D. N. Baxter, M. Boffito, D. Browne, F. Burns, D. R. Chadwick, R.
677 Clark, C. Cosgrove, J. Galloway, A. L. Goodman, A. Heer, A. Higham, S. Iyengar, A. Jamal, C.
678 Jeanes, P. A. Kalra, C. Kyriakidou, D. F. McAuley, A. Meyrick, A. M. Minassian, J. Minton, P.
679 Moore, I. Munsoor, H. Nicholls, O. Osanlou, J. Packham, C. H. Pretswell, A. S. F. Ramos, D.
680 Saralaya, R. P. Sheridan, R. Smith, R. L. Soiza, P. A. Swift, E. C. Thomson, J. Turner, M. E.
681 Viljoen, G. Albert, I. Cho, F. Dubovsky, G. Glenn, J. Rivers, A. Robertson, K. Smith, S. Toback,
682 2019nCoV-302 Study Group, Safety and Efficacy of NVX-CoV2373 Covid-19 Vaccine. *N.
683 Engl. J. Med.* **385**, NEJMoa2107659 (2021).
- 684 25. M. Silva, Y. Kato, M. B. Melo, I. Phung, B. L. Freeman, Z. Li, K. Roh, J. W. V. Wijnbergen,
685 H. Watkins, C. A. Enemuo, B. L. Hartwell, J. Y. H. Chang, S. Xiao, K. A. Rodrigues, K. M.
686 Cirelli, N. Li, S. Haupt, A. Aung, B. Cossette, W. Abraham, S. Kataria, R. Bastidas, J. Bhiman,
687 C. Linde, N. I. Bloom, B. Groschel, E. Georgeson, N. Phelps, A. Thomas, J. Bals, D. G.
688 Carnathan, D. Lingwood, D. R. Burton, G. Alter, T. P. Padera, A. M. Belcher, W. R. Schief, G.
689 Silvestri, R. M. Ruprecht, S. Crotty, D. J. Irvine, A particulate saponin/TLR agonist vaccine
690 adjuvant alters lymph flow and modulates adaptive immunity. *Science immunology* **6**, eabf1152
691 (2021).
- 692 26. H. B. Gristick, H. Hartweger, M. Loewe, J. van Schooten, V. Ramos, T. Y. Oliveira, Y.
693 Nishimura, N. S. Koranda, A. Wall, K.-H. Yao, D. Poston, A. Gazumyan, M. Wiatr, M. Horning,
694 J. R. Keeffe, M. A. G. Hoffmann, Z. Yang, M. E. Abernathy, K.-M. A. Dam, H. Gao, P. N. P.
695 Gnanapragasam, L. M. Kakutani, A. J. Pavlovitch-Bedzyk, M. S. Seaman, M. Howarth, A. T.
696 McGuire, L. Stamatatos, M. A. Martin, A. P. WestJr., M. C. Nussenzweig, P. J. Bjorkman, CD4
697 binding site immunogens elicit heterologous anti-HIV-1 neutralizing antibodies in transgenic
698 and wild-type animals. *Sci. Immunol.* **8**, eade6364 (2023).

- 699 27. D. W. Kulp, J. M. Steichen, M. Pauthner, X. Hu, T. Schiffner, A. Liguori, C. A. Cottrell, C.
700 Havenar-Daughton, G. Ozorowski, E. Georgeson, O. Kalyuzhnii, J. R. Willis, M. Kubitz, Y.
701 Adachi, S. M. Reiss, M. Shin, N. de Val, A. B. Ward, S. Crotty, D. R. Burton, W. R. Schief,
702 Structure-based design of native-like HIV-1 envelope trimers to silence non-neutralizing
703 epitopes and eliminate CD4 binding. *Nat. Commun.* **8**, 1655 (2017).
- 704 28. T. M. Gierahn, M. H. Wadsworth, T. K. Hughes, B. D. Bryson, A. Butler, R. Satija, S.
705 Fortune, J. C. Love, A. K. Shalek, Seq-Well: portable, low-cost RNA sequencing of single cells
706 at high throughput. *Nature methods* **14**, 395–398 (2017).
- 707 29. T. K. Hughes, M. H. Wadsworth, T. M. Gierahn, T. Do, D. Weiss, P. R. Andrade, F. Ma, B.
708 J. de A. Silva, S. Shao, L. C. Tsoi, J. Ordovas-Montanes, J. E. Gudjonsson, R. L. Modlin, J. C.
709 Love, A. K. Shalek, Second-Strand Synthesis-Based Massively Parallel scRNA-Seq Reveals
710 Cellular States and Molecular Features of Human Inflammatory Skin Pathologies. *Immunity* **53**,
711 878-894.e7 (2020).
- 712 30. D. M. Morgan, Y. Zhang, J.-H. Kim, M. Murillo, S. Singh, J. Loschko, N. Surendran, S. U.
713 Patil, I. Kanevsky, L. Chorro, J. C. Love, Full-length single-cell BCR sequencing paired with
714 RNA sequencing reveals convergent responses to vaccination. *bioRxiv* , 2023.05.23.541927
715 (2023).
- 716 31. K. L. Calame, Plasma cells: finding new light at the end of B cell development. *Nat.*
717 *Immunol.* **2**, 1103–1108 (2001).
- 718 32. D. Suan, N. J. Kräutler, J. L. V. Maag, D. Butt, K. Bourne, J. R. Hermes, D. T. Avery, C.
719 Young, A. Statham, M. Elliott, M. E. Dinger, A. Basten, S. G. Tangye, R. Brink, CCR6 Defines
720 Memory B Cell Precursors in Mouse and Human Germinal Centers, Revealing Light-Zone
721 Location and Predominant Low Antigen Affinity. *Immunity* **47**, 1142-1153.e4 (2017).
- 722 33. B. J. Laidlaw, L. Duan, Y. Xu, S. E. Vazquez, J. G. Cyster, The transcription factor Hhex
723 cooperates with the corepressor Tle3 to promote memory B cell development. *Nature*
724 *immunology* **21**, 1082–1093 (2020).
- 725 34. B. J. Laidlaw, J. G. Cyster, Transcriptional regulation of memory B cell differentiation.
726 *Nature Reviews Immunology* **21**, 209–220 (2021).
- 727 35. N. S. D. Silva, U. Klein, Dynamics of B cells in germinal centres. *Nature Reviews*
728 *Immunology* **2015** *15*:3 **15**, 137–148 (2015).
- 729 36. D. Morgan, V. Tergaonkar, Unraveling B cell trajectories at single cell resolution. *Trends in*
730 *Immunology* **43**, 210–229 (2022).
- 731 37. R. A. Mitchell, H. Liao, J. Chesney, G. Fingerle-Rowsor, J. Baugh, J. David, R. Bucala,
732 Macrophage migration inhibitory factor (MIF) sustains macrophage proinflammatory function
733 by inhibiting p53: Regulatory role in the innate immune response. *Proceedings of the National*
734 *Academy of Sciences of the United States of America* **99**, 345–350 (2002).

- 735 38. A. M. McGee, D. L. Douglas, Y. Liang, S. M. Hyder, C. P. Baines, The mitochondrial
736 protein C1qbp promotes cell proliferation, migration and resistance to cell death. *Cell Cycle* **10**,
737 4119 (2011).
- 738 39. P. Pérez-Durán, L. Belver, V. G. de Yébenes, P. Delgado, D. G. Pisano, A. R. Ramiro, UNG
739 shapes the specificity of AID-induced somatic hypermutation. *The Journal of Experimental*
740 *Medicine* **209**, 1379 (2012).
- 741 40. P. C. Fernandez, S. R. Frank, L. Wang, M. Schroeder, S. Liu, J. Greene, A. Cocito, B. Amati,
742 Genomic targets of the human c-Myc protein. *Genes Dev.* **17**, 1115–1129 (2003).
- 743 41. A. B. Holmes, C. Corinaldesi, Q. Shen, R. Kumar, N. Compagno, Z. Wang, M. Nitzan, E.
744 Grunstein, L. Pasqualucci, R. Dalla-Favera, K. Basso, Single-cell analysis of germinal-center B
745 cells informs on lymphoma cell of origin and outcome. *J. Exp. Med.* **217**, e20200483 (2020).
- 746 42. H. W. King, N. Orban, J. C. Riches, A. J. Clear, G. Warnes, S. A. Teichmann, L. K. James,
747 Single-cell analysis of human B cell maturation predicts how antibody class switching shapes
748 selection dynamics. *Sci. Immunol.* **6**, 6291 (2021).
- 749 43. N. R. Mathew, J. K. Jayanthan, I. V. Smirnov, J. L. Robinson, H. Axelsson, S. S. Nakka, A.
750 Emmanouilidi, P. Czarnewski, W. T. Yewdell, K. Schön, C. Lebrero-Fernández, V. Bernasconi,
751 W. Rodin, A. M. Harandi, N. Lycke, N. Borcherding, J. W. Yewdell, V. Greiff, M. Bemark, D.
752 Angeletti, Single-cell BCR and transcriptome analysis after influenza infection reveals
753 spatiotemporal dynamics of antigen-specific B cells. *Cell reports* **35** (2021),
754 doi:10.1016/j.celrep.2021.109286.
- 755 44. A. D. Gitlin, Z. Shulman, M. C. Nussenzweig, Clonal selection in the germinal centre by
756 regulated proliferation and hypermutation. *Nature* **2014** *509*:7502 **509**, 637–640 (2014).
- 757 45. J. Pae, J. Ersching, T. B. R. Castro, M. Schips, L. Mesin, S. J. Allon, J. Ordovas-Montanes,
758 C. Mlynarczyk, A. Melnick, A. Efeyan, A. K. Shalek, M. Meyer-Hermann, G. D. Victora, Cyclin
759 D3 drives inertial cell cycling in dark zone germinal center B cells. *Journal of Experimental*
760 *Medicine* **218** (2021), doi:10.1084/jem.20201699/211603.
- 761 46. S. Finkin, H. Hartweger, T. Y. Oliveira, E. E. Kara, M. C. Nussenzweig, Protein Amounts of
762 the MYC Transcription Factor Determine Germinal Center B Cell Division Capacity. *Immunity*
763 **51**, 324-336.e5 (2019).
- 764 47. J. Ersching, A. Efeyan, L. Mesin, J. T. Jacobsen, G. Pasqual, B. C. Grabiner, D. Dominguez-
765 Sola, D. M. Sabatini, G. D. Victora, Germinal Center Selection and Affinity Maturation Require
766 Dynamic Regulation of mTORC1 Kinase. *Immunity* **46**, 1045-1058.e6 (2017).
- 767 48. M. Schuhmacher, F. Kohlhuber, M. Hözel, C. Kaiser, H. Burtscher, M. Jarsch, G. W.
768 Bornkamm, G. Laux, A. Polack, U. H. Weidle, D. Eick, The transcriptional program of a human
769 B cell line in response to Myc. *Nucleic Acids Res.* **29**, 397–406 (2001).

- 770 49. T. Peng, T. R. Golub, D. M. Sabatini, The Immunosuppressant Rapamycin Mimics a
771 Starvation-Like Signal Distinct from Amino Acid and Glucose Deprivation. *Mol. Cell. Biol.* **22**,
772 5575–5584 (2002).
- 773 50. P. Ramezani-Rad, C. Chen, Z. Zhu, R. C. Rickert, Cyclin D3 Governs Clonal Expansion of
774 Dark Zone Germinal Center B Cells. *Cell Reports* **33**, 108403 (2020).
- 775 51. E. C. Pielou, The measurement of diversity in different types of biological collections. *J.
776 Theor. Biol.* **13**, 131–144 (1966).
- 777 52. J. Chiffelle, R. Genolet, M. A. Perez, G. Coukos, V. Zoete, A. Harari, T-cell repertoire
778 analysis and metrics of diversity and clonality. *Curr. Opin. Biotechnol.* **65**, 284–295 (2020).
- 779 53. C. E. Shannon, A Mathematical Theory of Communication. *Bell System Technical Journal*
780 **27**, 379–423 (1948).
- 781 54. T. Tokatlian, B. J. Read, C. A. Jones, D. W. Kulp, S. Menis, J. Y. H. Chang, J. M. Steichen,
782 S. Kumari, J. D. Allen, E. L. Dane, A. Liguori, M. Sangesland, D. Lingwood, M. Crispin, W. R.
783 Schief, D. J. Irvine, Innate immune recognition of glycans targets HIV nanoparticle immunogens
784 to germinal centers. *Science* **363**, 649–654 (2019).
- 785 55. B. J. Read, L. Won, J. C. Kraft, I. Sappington, A. Aung, S. Wu, J. Bals, C. Chen, K. K. Lee,
786 D. Lingwood, N. P. King, D. J. Irvine, Mannose-binding lectin and complement mediate
787 follicular localization and enhanced immunogenicity of diverse protein nanoparticle
788 immunogens. *Cell Rep.* **38**, 110217–110217 (2022).
- 789 56. J. T. Martin, C. A. Cottrell, A. Antanasijevic, D. G. Carnathan, B. J. Cossette, C. A. Enemuo,
790 E. H. Gebru, Y. Choe, F. Viviano, S. Fischinger, T. Tokatlian, K. M. Cirelli, G. Ueda, J. Coppins,
791 T. Schiffner, S. Menis, G. Alter, W. R. Schief, S. Crotty, N. P. King, D. Baker, G. Silvestri, A.
792 B. Ward, D. J. Irvine, Targeting HIV Env immunogens to B cell follicles in nonhuman primates
793 through immune complex or protein nanoparticle formulations. *Npj Vaccines* **5**, 72 (2020).
- 794 57. A. Aung, A. Cui, L. Maiorino, A. P. Amini, J. R. Gregory, M. Bukenya, Y. Zhang, H. Lee,
795 C. A. Cottrell, D. M. Morgan, M. Silva, H. Suh, J. D. Kirkpatrick, P. Amlashi, T. Remba, L. M.
796 Froehle, S. Xiao, W. Abraham, J. Adams, J. C. Love, P. Huyett, D. S. Kwon, N. Hacohen, W. R.
797 Schief, S. N. Bhatia, D. J. Irvine, Low protease activity in B cell follicles promotes retention of
798 intact antigens after immunization. *Science* **379** (2023), doi:10.1126/science.abn8934.
- 799 58. S. Ols, K. Lenart, R. A. Cerveira, M. C. Miranda, N. Brunette, J. Kochmann, M. Corcoran,
800 R. Skotheim, A. Philomin, A. Cagigi, B. Fiala, S. Wrenn, J. Marcandalli, F. Hellgren, E. A.
801 Thompson, A. Lin, F. Gegenfurtner, A. Kumar, M. Chen, G. E. Phad, B. S. Graham, L. Perez, A.
802 J. Borst, G. B. K. Hedestam, T. J. Ruckwardt, N. P. King, K. Loré, Multivalent antigen display
803 on nanoparticle immunogens increases B cell clonotype diversity and neutralization breadth to
804 pneumoviruses. *Immunity* (2023), doi:10.1016/j.jimmuni.2023.08.011.

- 805 59. Y. Kato, R. K. Abbott, B. L. Freeman, S. Haupt, B. Groschel, M. Silva, S. Menis, D. J.
806 Irvine, W. R. Schief, S. Crotty, Multifaceted Effects of Antigen Valency on B Cell Response
807 Composition and Differentiation In Vivo. *Immunity* **53**, 548–563.e8 (2020).
- 808 60. B. Shi, L. Ma, X. He, X. Wang, P. Wang, L. Zhou, X. Yao, Comparative analysis of human
809 and mouse immunoglobulin variable heavy regions from IMGT/LIGM-DB with IMGT/HighV-
810 QUEST. *Theor. Biol. Méd. Model.* **11**, 30 (2014).
- 811 61. R. K. Abbott, S. Crotty, Factors in B cell competition and immunodominance. *Immunol Rev*
812 **296**, 120–131 (2020).
- 813 62. W. Norde, Adsorption of proteins from solution at the solid-liquid interface. *Adv. Colloid
814 Interface Sci.* **25**, 267–340 (1986).
- 815 63. M. Rabe, D. Verdes, S. Seeger, Understanding protein adsorption phenomena at solid
816 surfaces. *Adv Colloid Interfac* **162**, 87–106 (2011).
- 817 64. S. L. Hem, H. HogenEsch, C. R. Middaugh, D. B. Volkin, Preformulation studies—The next
818 advance in aluminum adjuvant-containing vaccines. *Vaccine* **28**, 4868–4870 (2010).
- 819 65. A. Colaprico, S. Senesi, F. Ferlicca, B. Brunelli, M. Uguzzoli, M. Pallaoro, D. T. O'Hagan,
820 Adsorption onto aluminum hydroxide adjuvant protects antigens from degradation. *Vaccine* **38**,
821 3600–3609 (2020).
- 822 66. S. W. de Taeye, G. Ozorowski, A. Torrents de la Peña, M. Guttman, J.-P. Julien, T. L. G. M.
823 van den Kerkhof, J. A. Burger, L. K. Pritchard, P. Pugach, A. Yasmeen, J. Crampton, J. Hu, I.
824 Bontjer, J. L. Torres, H. Arendt, J. DeStefano, W. C. Koff, H. Schuitemaker, D. Eggink, B.
825 Berkhouit, H. Dean, C. LaBranche, S. Crotty, M. Crispin, D. C. Montefiori, P. J. Klasse, K. K.
826 Lee, J. P. Moore, I. A. Wilson, A. B. Ward, R. W. Sanders, Immunogenicity of Stabilized HIV-1
827 Envelope Trimers with Reduced Exposure of Non-neutralizing Epitopes. *Cell* **163**, 1702–1715
828 (2015).
- 829 67. B. A. Heesters, P. Chatterjee, Y.-A. Kim, S. F. Gonzalez, M. P. Kuligowski, T. Kirchhausen,
830 M. C. Carroll, Endocytosis and Recycling of Immune Complexes by Follicular Dendritic Cells
831 Enhances B Cell Antigen Binding and Activation. *Immunity* **38**, 1164–1175 (2013).
- 832 68. T. G. Phan, I. Grigorova, T. Okada, J. G. Cyster, Subcapsular encounter and complement-
833 dependent transport of immune complexes by lymph node B cells. *Nat Immunol* **8**, 992–1000
834 (2007).
- 835 69. F. D. Batista, N. E. Harwood, The who, how and where of antigen presentation to B cells.
836 *Nat Rev Immunol* **9**, 15–27 (2009).
- 837 70. J. Kranich, N. J. Krautler, How Follicular Dendritic Cells Shape the B-Cell Antigenome.
838 *Front Immunol* **7**, 225 (2016).

- 839 71. C. Park, J. Arthos, C. Cicala, J. H. Kehrl, The HIV-1 envelope protein gp120 is captured and
840 displayed for B cell recognition by SIGN-R1(+) lymph node macrophages. *Elife* **4**:e06467
841 (2015), doi:10.7554/elife.06467.
- 842 72. Y. R. Carrasco, F. D. Batista, B Cells Acquire Particulate Antigen in a Macrophage-Rich
843 Area at the Boundary between the Follicle and the Subcapsular Sinus of the Lymph Node.
844 *Immunity* **27**, 160–171 (2007).
- 845 73. T. G. Phan, J. A. Green, E. E. Gray, Y. Xu, J. G. Cyster, Immune complex relay by
846 subcapsular sinus macrophages and noncognate B cells drives antibody affinity maturation. *Nat.*
847 *Immunol.* **10**, 786–793 (2009).
- 848 74. T. Junt, E. A. Moseman, M. Iannaccone, S. Massberg, P. A. Lang, M. Boes, K. Fink, S. E.
849 Henrickson, D. M. Shayakhmetov, N. C. D. Paolo, N. van Rooijen, T. R. Mempel, S. P. Whelan,
850 U. H. von Andrian, Subcapsular sinus macrophages in lymph nodes clear lymph-borne viruses
851 and present them to antiviral B cells. *Nature* **450**, 110–114 (2007).
- 852 75. V. D. Ramanathan, P. Badenoch-Jones, J. L. Turk, Complement activation by aluminium and
853 zirconium compounds. *Immunology* **37**, 881–8 (1979).
- 854 76. E. Güven, K. Duus, I. Laursen, P. Højrup, G. Houen, Aluminum Hydroxide Adjuvant
855 Differentially Activates the Three Complement Pathways with Major Involvement of the
856 Alternative Pathway. *Plos One* **8**, e74445 (2013).
- 857 77. P. J. Klasse, T. J. Ketas, C. A. Cottrell, G. Ozorowski, G. Debnath, D. Camara, E.
858 Francomano, P. Pugach, R. P. Ringe, C. C. LaBranche, M. J. van Gils, C. A. Bricault, D. H.
859 Barouch, S. Crotty, G. Silvestri, S. Kasturi, B. Pulendran, I. A. Wilson, D. C. Montefiori, R. W.
860 Sanders, A. B. Ward, J. P. Moore, Epitopes for neutralizing antibodies induced by HIV-1
861 envelope glycoprotein BG505 SOSIP trimers in rabbits and macaques. *PLoS Pathog.* **14**,
862 e1006913 (2018).
- 863 78. L. E. McCoy, M. J. van Gils, G. Ozorowski, T. Messmer, B. Briney, J. E. Voss, D. W. Kulp,
864 M. S. Macauley, D. Sok, M. Pauthner, S. Menis, C. A. Cottrell, J. L. Torres, J. Hsueh, W. R.
865 Schief, I. A. Wilson, A. B. Ward, R. W. Sanders, D. R. Burton, Holes in the Glycan Shield of the
866 Native HIV Envelope Are a Target of Trimer-Elicited Neutralizing Antibodies. *Cell Rep.* **16**,
867 2327–2338 (2016).
- 868 79. J. Jardine, J.-P. Julien, S. Menis, T. Ota, O. Kalyuzhnii, A. McGuire, D. Sok, P.-S. Huang, S.
869 MacPherson, M. Jones, T. Nieusma, J. Mathison, D. Baker, A. B. Ward, D. R. Burton, L.
870 Stamatatos, D. Nemazee, I. A. Wilson, W. R. Schief, Rational HIV Immunogen Design to Target
871 Specific Germline B Cell Receptors. *Science* **340**, 711–716 (2013).
- 872 80. B. Kaminow, D. Yunusov, A. Dobin, STARSolo: accurate, fast and versatile
873 mapping/quantification of single-cell and single-nucleus RNA-seq data. (2021),
874 doi:10.1101/2021.05.05.442755.

- 875 81. Y. Hao, S. Hao, E. Andersen-Nissen, W. M. Mauck, S. Zheng, A. Butler, M. J. Lee, A. J.
876 Wilk, C. Darby, M. Zager, P. Hoffman, M. Stoeckius, E. Papalexi, E. P. Mimitou, J. Jain, A.
877 Srivastava, T. Stuart, L. M. Fleming, B. Yeung, A. J. Rogers, J. M. McElrath, C. A. Blish, R.
878 Gottardo, P. Smibert, R. Satija, Integrated analysis of multimodal single-cell data. *Cell* **184**,
879 3573–3587.e29 (2021).
- 880 82. P. Roelli, bbimber, B. Flynn, santiagoreviale, G. Gui, Hoohm/CITE-seq-Count: 1.4.2. (2019),
881 doi:10.5281/zenodo.2590196.
- 882 83. F. A. Wolf, P. Angerer, F. J. Theis, SCANPY: Large-scale single-cell gene expression data
883 analysis. *Genome Biology* **19**, 1–5 (2018).
- 884 84. V. Bergen, M. Lange, S. Peidli, F. A. Wolf, F. J. Theis, Generalizing RNA velocity to
885 transient cell states through dynamical modeling. *Nature Biotechnology* **2020** *38*:12 **38**, 1408–
886 1414 (2020).
- 887 85. T. Tiller, E. Meffre, S. Yurasov, M. Tsuiji, M. C. Nussenzweig, H. Wardemann, Efficient
888 generation of monoclonal antibodies from single human B cells by single cell RT-PCR and
889 expression vector cloning. *Journal of Immunological Methods* **329**, 112–124 (2008).
- 890 86. J. A. V. Heiden, G. Yaari, M. Uduman, J. N. H. Stern, K. C. O’Connor, D. A. Hafler, F.
891 Vigneault, S. H. Kleinstein, pRESTO: a toolkit for processing high-throughput sequencing raw
892 reads of lymphocyte receptor repertoires. *Bioinformatics (Oxford, England)* **30**, 1930–1932
893 (2014).
- 894 87. N. T. Gupta, J. A. V. Heiden, M. Uduman, D. Gadala-Maria, G. Yaari, S. H. Kleinstein,
895 Change-O: A toolkit for analyzing large-scale B cell immunoglobulin repertoire sequencing data.
896 *Bioinformatics* **31**, 3356–3358 (2015).
- 897 88. T. Smith, A. Heger, I. Sudbery, UMI-tools: modeling sequencing errors in Unique Molecular
898 Identifiers to improve quantification accuracy. *Genome research* **27**, 491–499 (2017).
- 899 89. J. Ye, N. Ma, T. L. Madden, J. M. Ostell, IgBLAST: an immunoglobulin variable domain
900 sequence analysis tool. *Nucleic Acids Research* **41**, W34 (2013).
- 901 90. Z. Gu, L. Gu, R. Eils, M. Schlesner, B. Brors, circlize Implements and enhances circular
902 visualization in R. *Bioinformatics (Oxford, England)* **30**, 2811–2812 (2014).
- 903 91. R. W. Sanders, R. Derking, A. Cupo, J.-P. Julien, A. Yasmeen, N. de Val, H. J. Kim, C.
904 Blattner, A. T. de la Peña, J. Korzun, M. Golabek, K. de los Reyes, T. J. Ketas, M. J. van Gils, C.
905 R. King, I. A. Wilson, A. B. Ward, P. J. Klasse, J. P. Moore, A Next-Generation Cleaved,
906 Soluble HIV-1 Env Trimer, BG505 SOSIP.664 gp140, Expresses Multiple Epitopes for Broadly
907 Neutralizing but Not Non-Neutralizing Antibodies. *PLoS Pathog.* **9**, e1003618 (2013).

- 908 92. C. Suloway, J. Pulokas, D. Fellmann, A. Cheng, F. Guerra, J. Quispe, S. Stagg, C. S. Potter,
909 B. Carragher, Automated molecular microscopy: The new Leginon system. *J. Struct. Biol.* **151**,
910 41–60 (2005).
- 911 93. G. C. Lander, S. M. Stagg, N. R. Voss, A. Cheng, D. Fellmann, J. Pulokas, C. Yoshioka, C.
912 Irving, A. Mulder, P.-W. Lau, D. Lyumkis, C. S. Potter, B. Carragher, Appion: An integrated,
913 database-driven pipeline to facilitate EM image processing. *J. Struct. Biol.* **166**, 95–102 (2009).

914

915 **Acknowledgments:** We thank the Koch Institute Robert A. Swanson (1969) BioMicro Center
916 and Biotechnology Center for technical support, specifically the Histology, Flow
917 Cytometry, and Microscopy cores. Select figures created with BioRender.com. DJI is an
918 investigator of the Howard Hughes Medical Institute.

919 **Funding:**

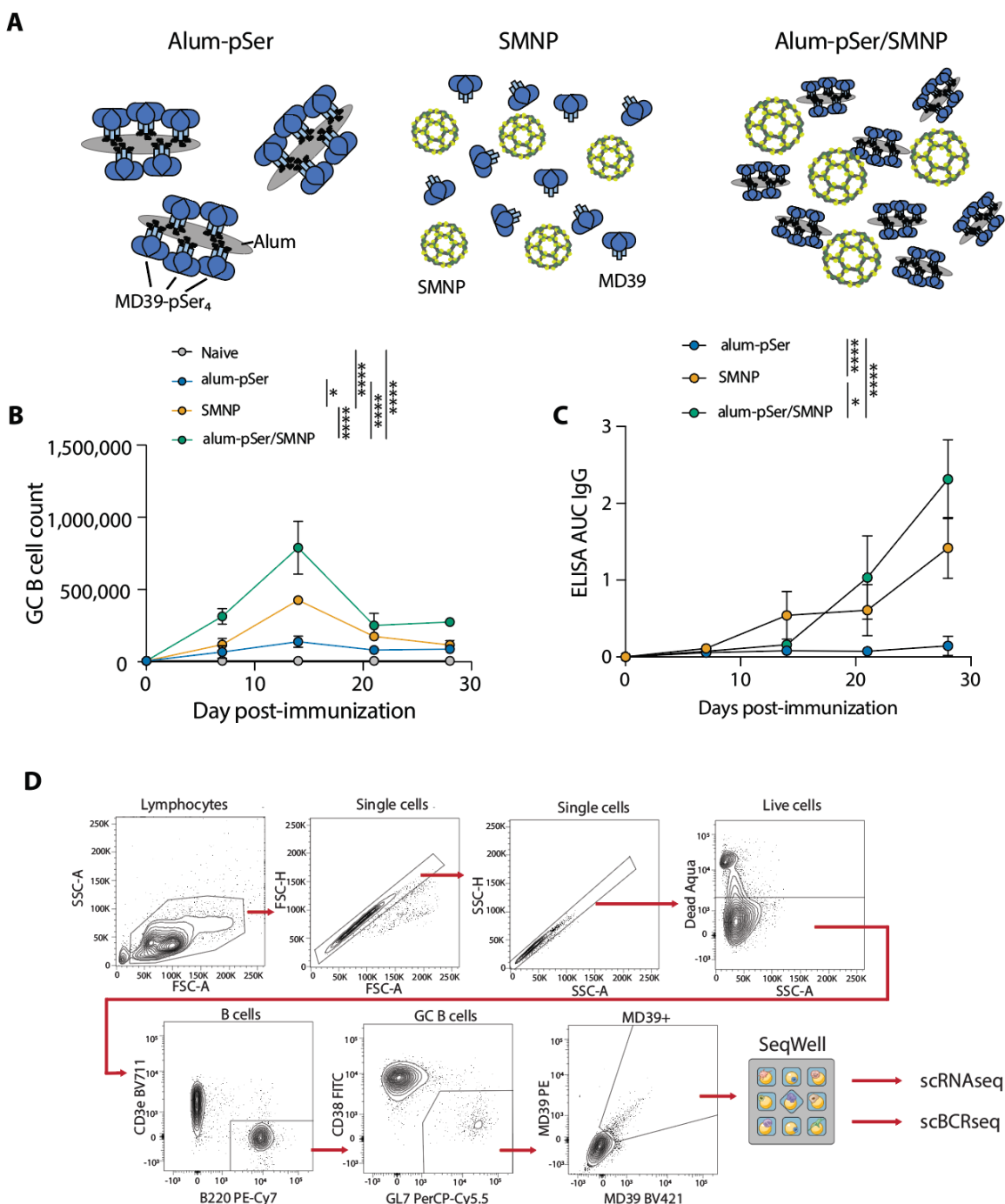
920 National Institutes of Health grant P30-CA14051 (Koch Institute Core grant)
921 National Institutes of Health grant UM1AI144462 (ABW, WRS, DJI)
922 National Institutes of Health grant AI161818 (DJI)
923 National Institutes of Health grant AI161297 (DJI)
924 National Institutes of Health grant AI125068 (DJI)
925 National Institutes of Health grant P01AI048240 (DJI)
926 Ragon Institute of MGH, MIT, and Harvard (DJI)
927 Howard Hughes Medical Institute (DJI)
928 National Institutes of Health Fellowship F32 AI164829 (PY)

929 **Author contributions:** KAR, YJZ, AA, DM, JCL, and DJI conceived the study plan. KAR
930 synthesized the pSer linkers and SMNP. WRS designed the antigen constructs. KAR
931 completed the in vitro characterization of the antigen constructs. YJZ and DM completed
932 cell sorting, sequencing, and sequencing analysis. KAR, AA, LM, PY, JRG, PA, and MB
933 completed the mouse studies. GG and GO completed the TEM imaging. KAR and AA
934 completed fluorescence imaging. KAR, YJZ, and DJI wrote the manuscript. All authors
935 reviewed and edited the manuscript. ABW, WRS, JCP, and DJI supervised the study.

936 **Competing interests:** DJI and WRS are named as an inventor on a patent for pSer technology
937 (US No. 11,224,648 B2). DJI is named as an inventor on a patent for SMNP (US No.
938 11,547,672). KAR and DJI are named as inventors on patent applications for an
939 engineered pSer-conjugated SARS-CoV-2 RBD (PCT/US22/74309 and US No.
940 17/816,061). KAR and DJI are named as inventors on patent applications for the
941 combination of alum and SMNP adjuvants (PCT/US2022/074302 and US No.
942 17/816,045). KAR, DJI, and WRS are named as inventors on patent applications for
943 MD39_nohis8_congly-pSer₄ design referenced in these studies as MD39-pSer₄ (US No.
944 63/500,068). All other authors declare they have no competing interests.

945 **Data and materials availability:** All data are available in the main text or the supplementary
946 materials.

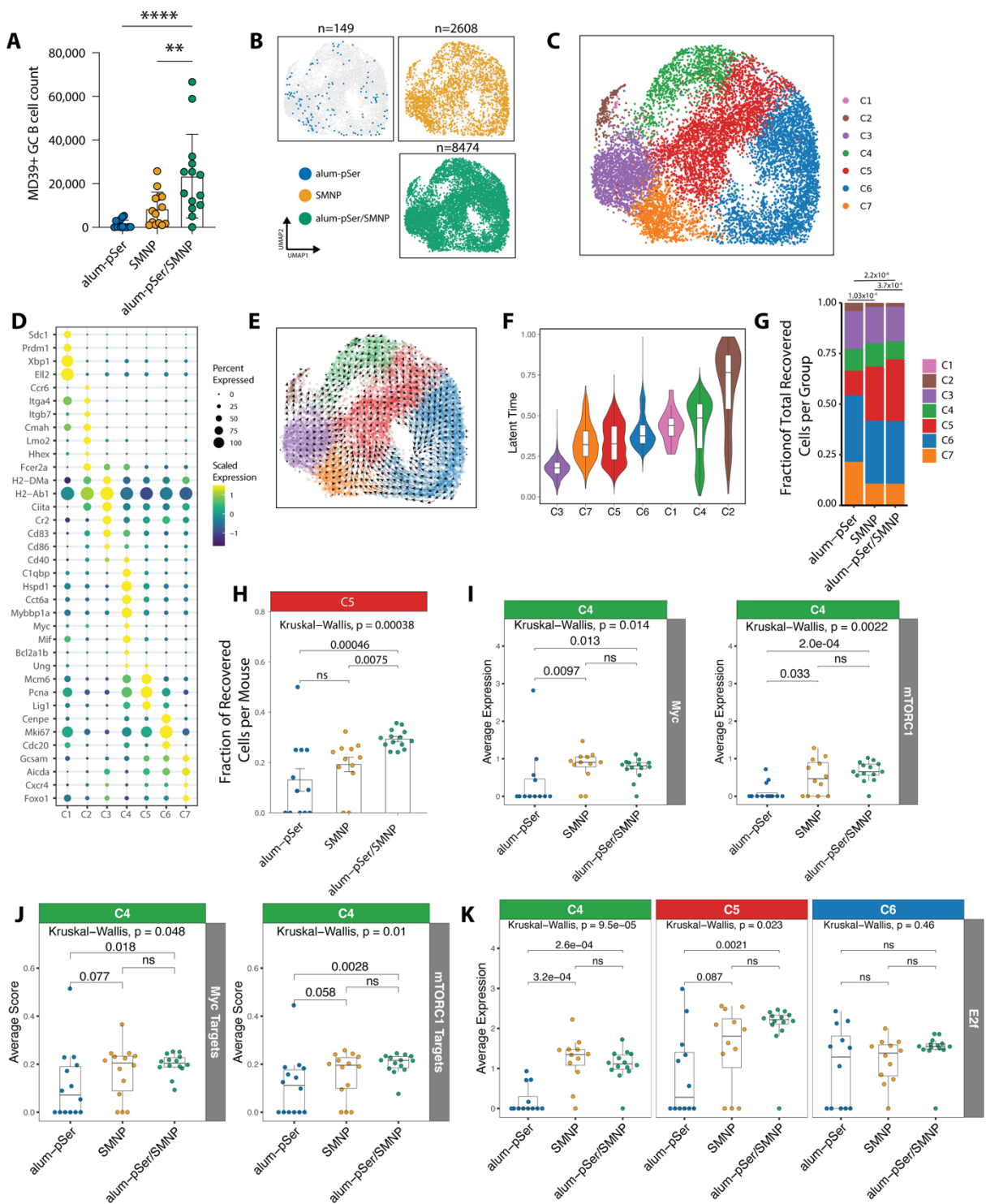
947 **Figures**



948

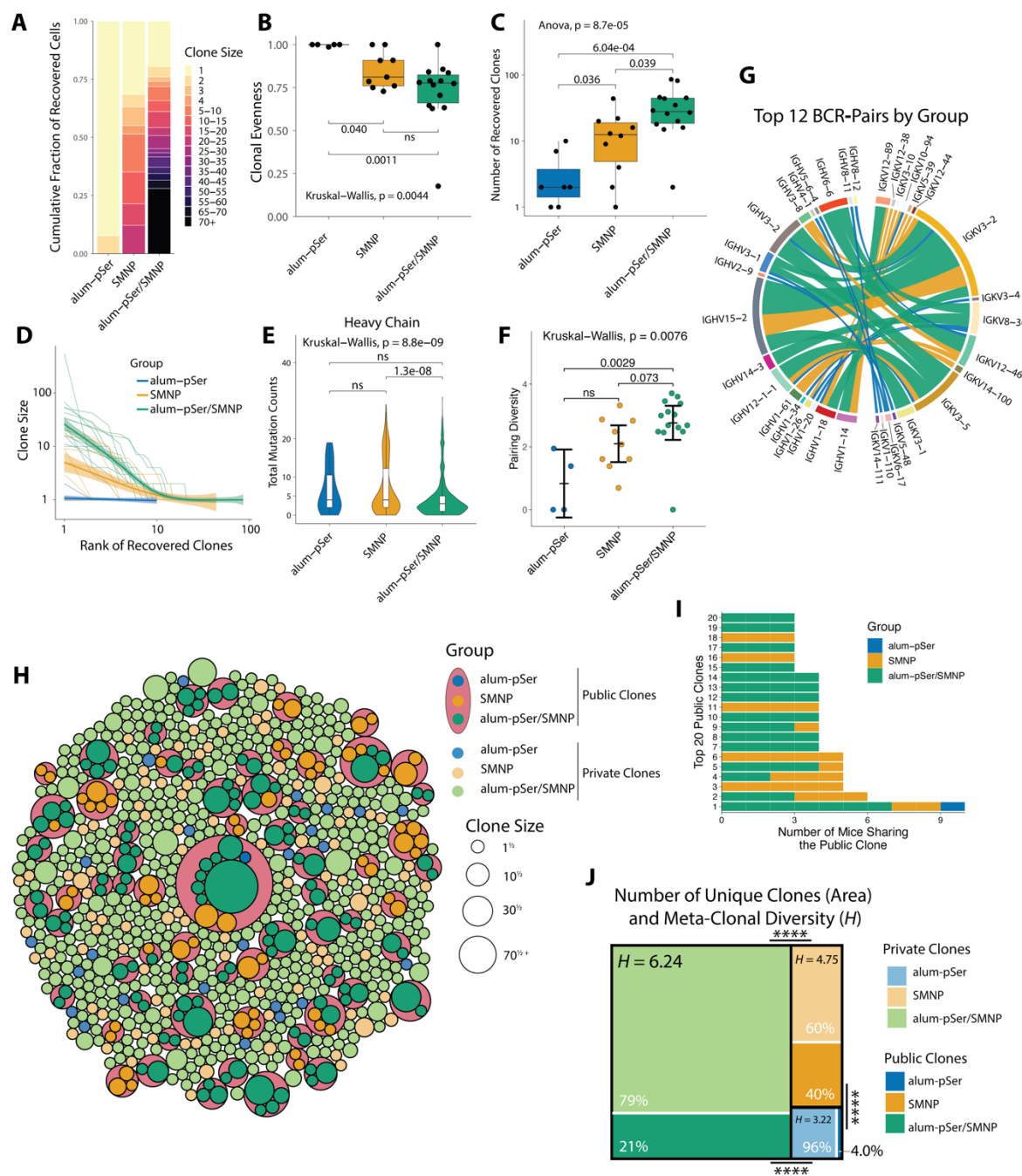
949 **Fig. 1. pSer-modified Env trimer anchored on alum combined with SMNP adjuvant**
950 **amplifies humoral immune responses.** (A) Schematic of immunization groups. (B–C) BALB/c
951 mice ($n=5$ /group for flow cytometry analysis, $n=14$ /group for scRNA-seq and scBCR-seq) were
952 immunized with 5 μ g MD39 Env trimer \pm 50 μ g alum \pm 5 μ g SMNP. (B) Total germinal center
953 (GC) B cell counts over time. Values plotted are mean \pm s.e.m. (C) Serum IgG antibody responses
954 were assessed longitudinally by ELISA using MD39 captured by lectin. Values plotted are ELISA
955 area under the curve (AUC) mean \pm s.d. (D) The GC responses in draining lymph nodes were

956 analyzed by flow cytometry, and MD39-binding GC B cells were loaded onto SeqWell arrays for
957 scRNA-seq and scBCR-seq. Statistical significance was determined by two-way ANOVA
958 followed by Tukey's multiple comparisons test. ns p>0.05, * p<0.05, ** p<0.01, *** p<0.001,
959 **** p<0.0001.



960
961 **Fig. 2. scRNA-seq profiling of MD39-binding germinal center B cells 14 days post-**
962 **immunization. (A)** GC B cell counts detected by flow cytometry and loaded onto SeqWell arrays.
963 Shown are mean \pm s.e.m. **(B)** UMAP projection of recovered cells by immunization group. Gray

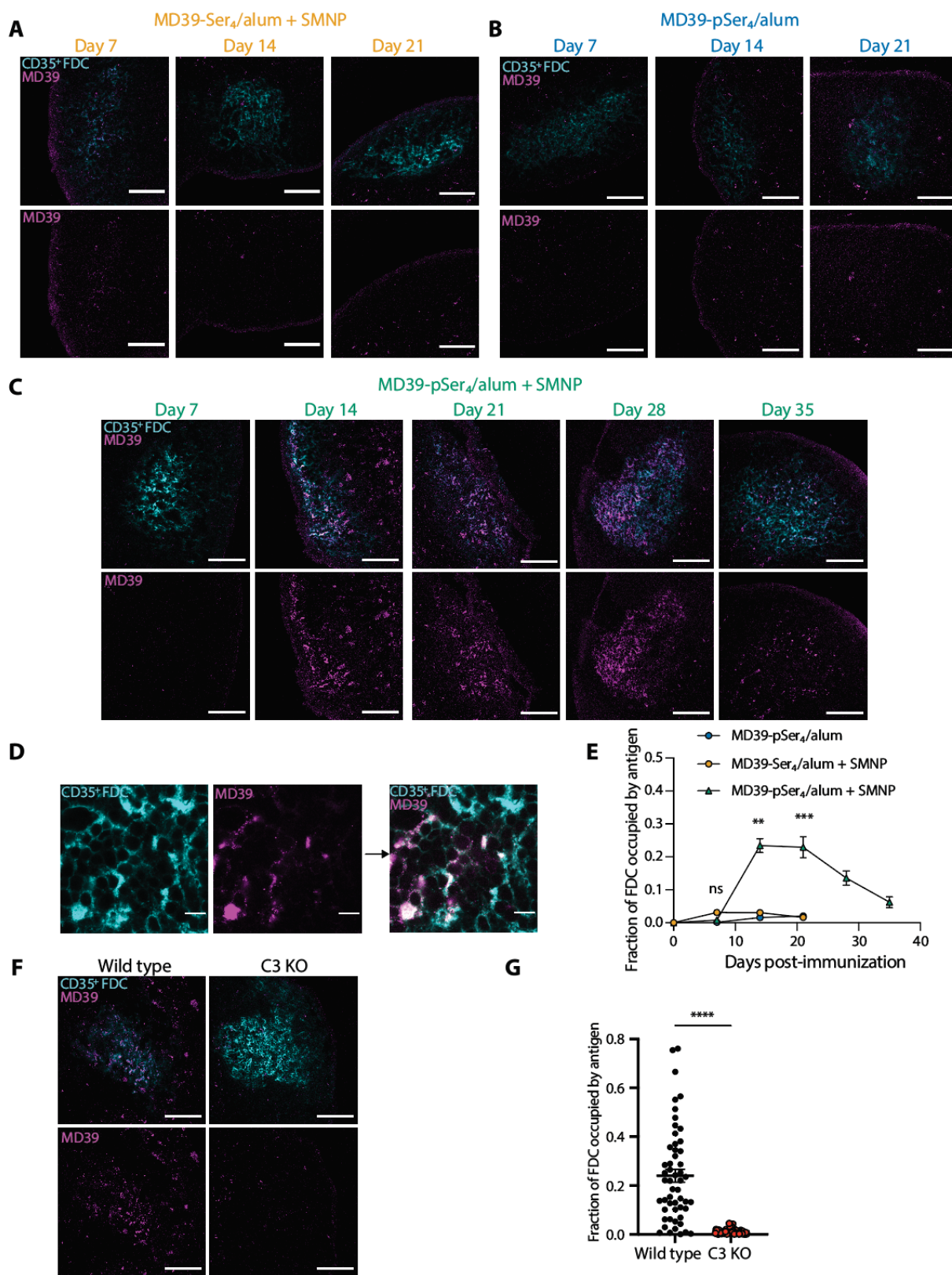
964 dots represent all recovered cells. (C) UMAP projection of phenotypic clusters of MD39-binding
965 GC B cells. (D) Differentially expressed genes associated with phenotypic clusters. The color
966 indicates scaled expression levels. The dot radius indicates the fraction of cells expressing the
967 gene. (E) UMAP projection of RNA velocity vector fields. The length of the arrows indicates the
968 speed of differentiation. (F) Latent time distribution by clusters. (G) Cluster distribution of
969 recovered cells. (H) The fraction of C5 cells per mouse from each vaccine group. (I) Average
970 expression of *Myc* and mTORC1 genes (sum of *Mtor*, *Rptor*, *Akt1s1*, and *Deptor*) among C4 cells.
971 (J) Average module score of *Myc*- and *mTORC1*-target genes among C4 cells. (K) Average
972 expression of activating *E2f*-family transcription factors (sum of *E2fl*, *E2f2*, *E2f3*) among C4,
973 C5, and C6 cells. Dots in H-K represent the average expression of individual mice. For (A),
974 statistical significance was determined by one-way ANOVA followed by Tukey's multiple
975 comparisons test. ns p>0.05, ** p<0.01, **** p<0.0001. For (G), p values are computed with Chi-
976 squared tests with Bonferroni correction. For (H-K), p values are computed with Kruskal-Wallis
977 analysis of variance followed by Dunn's post hoc test.



978
979
980
981

Fig. 3. scBCR-seq analysis of MD39-binding germinal center B cells 14 days post-immunization. (A) Clone size distributions in each vaccine group. (B) The clonal evenness score computed by Pielou's index. Only mice with recovered IgH sequences were included in the

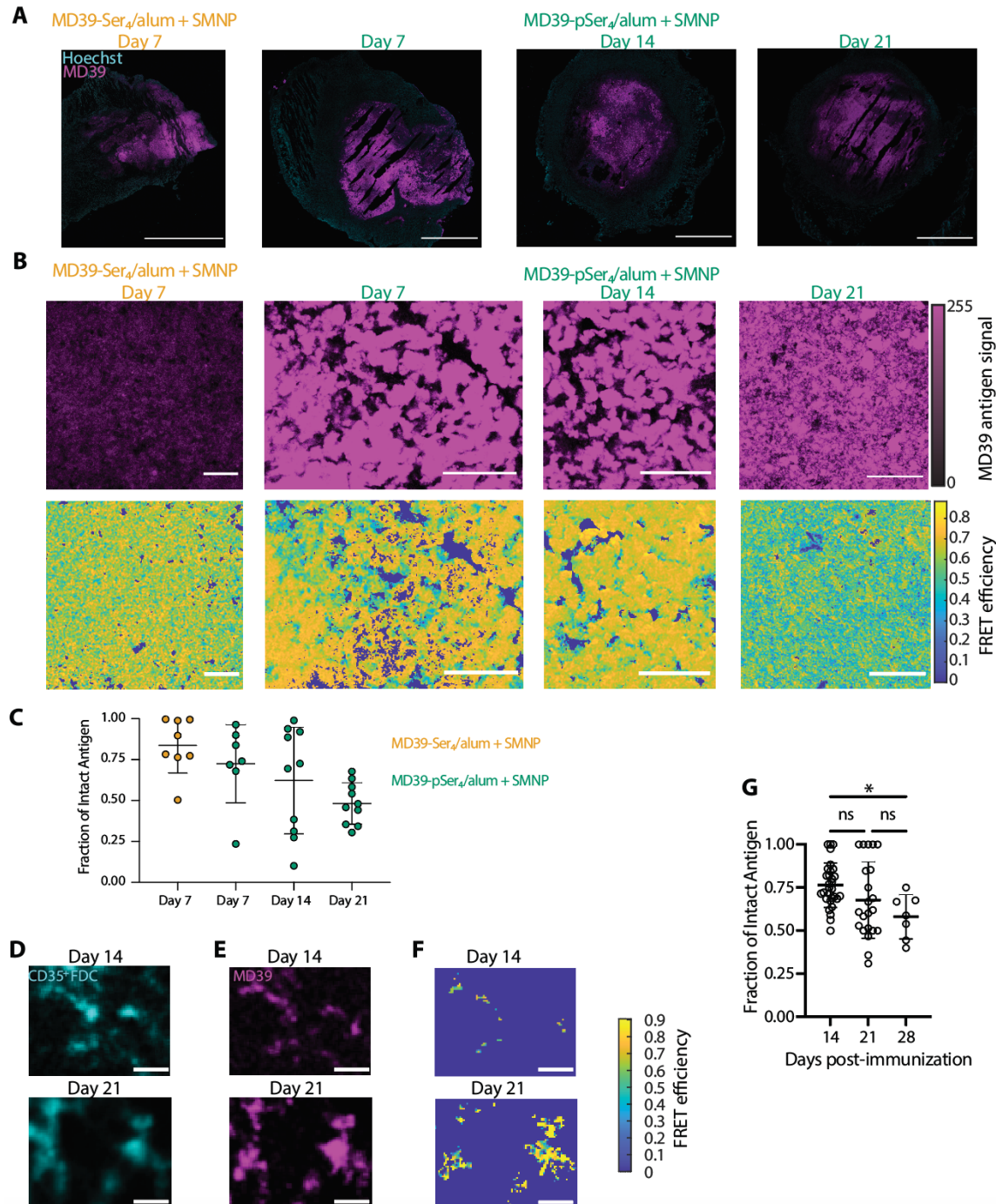
982 analysis. **(C)** Number of unique clones recovered per mouse across vaccine groups. Statistical
983 significance was determined by two-way ANOVA followed by Tukey's multiple comparisons test.
984 **(D)** Clone recovery curves for each immunization mouse. Spline regression models were fit for
985 each vaccine group. The shaded areas indicate 95% confidence intervals. **(E)** Heavy chain SHM
986 counts. **(F)** Clonal heavy and light chain V gene pairing diversity per mouse, calculated by the
987 Shannon diversity index. Shown are mean \pm s.e.m. **(G)** Top 12 BCR pairs from each vaccine group.
988 Each chord on the diagram represents one clone, and the colors indicate the vaccine groups. **(H)**
989 Recovered meta-clonotypes. Private clones are illustrated as individual circles in lighter colors.
990 Public clones are enclosed by coral-colored circles and illustrated in darker colors. The size of
991 each circle is proportional to the square root of clone sizes. **(I)** Top 20 public clones. **(J)** Treemap
992 illustration of meta-clonotypes. The areas of black-bordered boxes are proportional to the relative
993 numbers of recovered meta-clonotypes per group. The areas of inner boxes are proportional to the
994 percentage of private and public clones in each group. Meta-clonal diversity was labeled and
995 computed by Shannon's diversity index (H). Statistical significance for diversity indices was
996 determined by Hutcheson's t-test followed by Bonferroni multiple comparisons correction. ****
997 $p < 0.0001$. For **(B, E-F)**, p values were computed with Kruskal-Wallis analysis of variance
998 followed by Dunn's post hoc test.



999

1000 **Fig. 4. Env trimer antigen administered with alum anchoring and SMNP accumulates on the**
1001 **follicular dendritic cell network over time.** BALB/c mice ($n=3$ /group) were immunized with 10

1002 µg labeled MD39-Ser₄ (**A**) or MD39-pSer₄ (**B**) combined with 100 µg alum, or MD39-pSer₄
1003 combined with 100 µg alum and 5 µg SMNP (**C**). Draining inguinal lymph nodes were isolated at
1004 the indicated timepoints, flash frozen, and cryo-sectioned. Shown are representative images of
1005 antigen on the lymph node CD35⁺ follicular dendritic cell (FDC) networks. Overlay of antigen and
1006 FDC shown in top row of images, with antigen signal alone shown in the bottom row of images.
1007 Scale bars, 100 µm. (**D**) Shown are representative 100x objective lens images of CD35⁺ FDC
1008 staining and MD39 antigen, with overlay on right. Scale bars, 10 µm. (**E**) The fraction of FDCs
1009 occupied by antigen was calculated for each timepoint and immunization. Values plotted are mean
1010 ± s.e.m. Statistical significance was determined by one-way ANOVA followed by Tukey's
1011 multiple comparisons test. (**F**) Wild type C57BL/6 and C3 KO mice (*n*=3/group) were immunized
1012 with 10 µg labeled MD39-pSer₄ combined with 100 µg alum and 5 µg SMNP. Draining inguinal
1013 lymph nodes were isolated 14 days after immunization, flash frozen, and cryo-sectioned. Shown
1014 are representative images of antigen on the lymph node CD35⁺ follicular dendritic cell (FDC)
1015 networks. Overlay of antigen and FDC shown in top row of images, with antigen signal alone
1016 shown in the bottom row of images. Scale bars, 100 µm. (**G**) Fraction of FDCs occupied by antigen
1017 for each mouse strain. Values plotted are mean ± s.e.m. Statistical significance was determined by
1018 Mann Whitney test. ns p>0.05, * p<0.05, ** p<0.01, *** p<0.001, **** p<0.0001.



1019

1020 **Fig. 5. Env trimer antigen accumulated on FDCs following alum-pSer/SMNP immunization**
1021 **is highly intact.** (A) BALB/c mice ($n=3$ /group) were immunized with 10 μ g of FRET dye-labeled
1022 MD39-Ser₄ or MD39-pSer₄ combined with 100 μ g alum and 5 μ g SMNP. Injection sites were
1023 isolated at the indicated timepoints, flash frozen, and cryo-sectioned. Shown are representative
1024 images of antigen and Hoechst nuclei staining at the injection site. Scale bars represent 1000 μ m.
1025 (B) Representative pre-bleach acceptor images. These regions underwent acceptor
1026 photobleaching, enabling the calculation of FRET efficiencies, shown as a heatmap below. Scale
1027 bars, 50 μ m. (C) The fraction of intact antigen at the injection site was calculated based on the

1028 antigen FRET efficiencies. Values plotted are mean ± s.d. Representative (**D**) CD35⁺ FDC and (**E**)
1029 pre-bleach acceptor images in the draining lymph node FDC following immunization with MD39-
1030 pSer₄. Scale bars, 10 μm. These regions underwent acceptor photobleaching, enabling the
1031 calculation of FRET efficiencies, shown as a heatmap in (**F**). (**G**) The fraction of antigen that is
1032 intact in the follicles was calculated based on these FRET efficiencies. Values plotted are mean ±
1033 s.d. Statistical significance was determined by one-way ANOVA followed by Tukey's multiple
1034 comparisons test. ns p>0.05, * p<0.05, ** p<0.01, *** p<0.001, **** p<0.0001.